Cell Reports

Article

# Neuroinflammation induces aberrant activation of Wnt signaling in astrocytes and impairment of cholesterol homeostasis and myelin integrity

## Graphical abstract

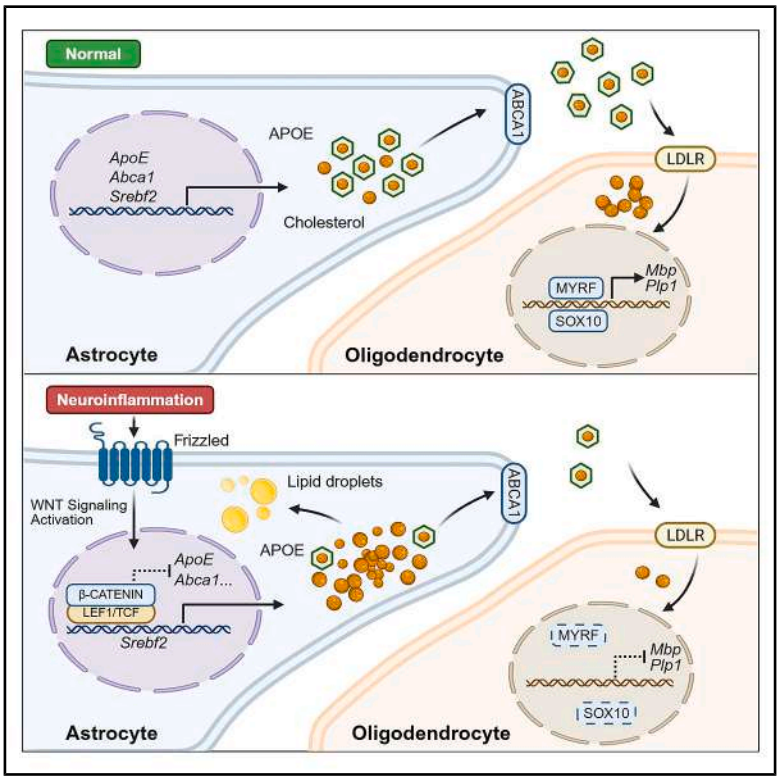


## Highlights

- Neuroinflammation activates Wnt signaling in astrocytes
- Wnt signaling upregulates SREBF2 and downregulates APOE in astrocytes
- Diminished APOE expression reduces cholesterol supply to oligodendrocytes
- Cholesterol deficiency impairs MYRF-dependent myelin gene expression

## Authors

Jiannan Zhang, Jiaru Zheng, Yi Ai, ..., Jingwei Zhao, Mengsheng Qiu, Kang Zheng

## Correspondence

msqiu@hznu.edu.cn (M.Q.), zhengkang@hznu.edu.cn (K.Z.)

## In brief

Zhang et al. show that neuroinflammation activates Wnt/β-CATENIN signaling in astrocytes, driving SREBF2-mediated cholesterol synthesis while suppressing APOE-dependent cholesterol efflux. The resulting reduction in cholesterol supply to oligodendrocytes impairs MYRF transcription factor activity and myelin gene expression, which may compromise myelin integrity.

Zhang et al., 2026, Cell Reports *45*, 117871
September 22, 2026 
https://doi.org/10.1016/j.celrep.2026.117871

CellPress

Cell Reports

CellPress
OPEN ACCESS

Article

# Neuroinflammation induces aberrant activation of Wnt signaling in astrocytes and impairment of cholesterol homeostasis and myelin integrity

Jiannan Zhang,[1] Jiaru Zheng,[1] Yi Ai,[1] Junlin Yang,[1] Cheng He,[2] Jingwei Zhao,[3] Mengsheng Qiu,[1,*] and Kang Zheng[1,4,*]
[1]Key Laboratory of Organ Development and Regeneration of Zhejiang Province, College of Life and Environment Sciences, Hangzhou Normal University, Hangzhou, Zhejiang 311121, China
[2]Institute of Neuroscience, Key Laboratory of Molecular Neurobiology of Ministry of Education, NMU, Shanghai 200433, China
[3]Department of Human Anatomy, Histology and Embryology, System Medicine Research Center, NHC and CAMS Key Laboratory of Medical Neurobiology, Zhejiang University School of Medicine, Hangzhou, Zhejiang 310058, China
[4]Lead contact
*Correspondence: msqiu@hznu.edu.cn (M.Q.), zhengkang@hznu.edu.cn (K.Z.)
https://doi.org/10.1016/j.celrep.2026.117871

## SUMMARY

Neuroinflammation often disrupts cerebral cholesterol homeostasis and leads to white matter damage and demyelination. However, the molecular mechanisms underlying these defects have remained enigmatic. In this study, we report that inflammation is associated with aberrant activation of Wnt signaling in astrocytes. While Wnt signaling increases astrocytic expression of SREBF2 protein and intracellular cholesterol level, it simultaneously inhibits the expression of APOE and reduces cholesterol efflux from astrocytes. The extracellular cholesterol supply is essential for the activation of the expression of MYRF transcription factor and myelin-associated genes in oligodendrocytes. Moreover, the defective oligodendrocyte differentiation and myelin gene expression caused by astrocytic Wnt activation in transgenic mice can partially be rescued by chemical-enhanced *ApoE* expression. Our findings suggest a regulatory pathway of "inflammation → Wnt signaling → cholesterol metabolism → myelin integrity" and provide important insights into the molecular mechanisms underlying inflammation-induced demyelinating diseases and future therapeutic strategies.

## INTRODUCTION

Neuroinflammation is a common feature of brain injury, stroke, and various neurodegenerative disorders. Recent studies demonstrated that neuroinflammation often disrupts cerebral cholesterol homeostasis and leads to white matter damage and demyelination.[1–3] Myelin formed by oligodendrocytes is highly enriched in cholesterol and phospholipids, providing electrical insulation for rapid conduction of nerve impulses along neuronal axons.[4] Damage to myelin integrity can directly lead to impaired neuronal electrical transmission, contributing to a spectrum of neurological disorders such as multiple sclerosis and leukodystrophies.[5] Despite the paramount importance of myelin structure in brain functioning, recent studies have demonstrated that myelin sheaths undergo constant turnover and new myelin is frequently added as a result of adaptive myelination.[6] However, oligodendrocytes possess limited capacity for cholesterol synthesis and must acquire approximately 80% of the cholesterol needed for myelin maintenance through uptake from the extracellular environment, mainly produced by astrocytes.[7–9] Thus, precise regulation of cholesterol biosynthesis and efflux has emerged as one of the core functions through which astrocytes contribute to central nervous system (CNS) homeostasis. Astrocytes serve as a major site of cholesterol synthesis in the brain, primarily via the Bloch pathway.[10] Meanwhile, astrocytes also express apolipoproteins, such as apolipoprotein E (APOE), to form lipoprotein complexes that supply cholesterol to neurons, oligodendrocytes, and other cell types.[11] This cholesterol transfer process involves precise coordination of cholesterol synthesis and efflux in astrocytes and uptake in oligodendrocytes.[8,9]

At this stage, little is known about the molecular mechanisms by which neuroinflammation impedes cholesterol synthesis and export in astrocytes and the associated myelin damage. Earlier studies identified Wnt/β-CATENIN signaling as a key regulator of lipid and cholesterol metabolism in peripheral tissues such as the liver and the endothelium.[12–14] Given that the Wnt/β-CATENIN pathway is often abnormally activated in inflammatory microenvironments,[15,16] it is plausible that neuroinflammation could induce Wnt activation, which impedes cholesterol synthesis in astrocytes and its supply to oligodendrocytes for myelin maintenance. Elucidating the functional link between Wnt signaling and cholesterol metabolism in astrocytes under inflammatory conditions is crucial for understanding the pathological mechanisms of inflammation-associated myelin injury.

Here, we report that lipopolysaccharide (LPS)-induced neuroinflammation triggered Wnt/β-CATENIN signaling, leading to increased cholesterol synthesis in astrocytes but repressed the

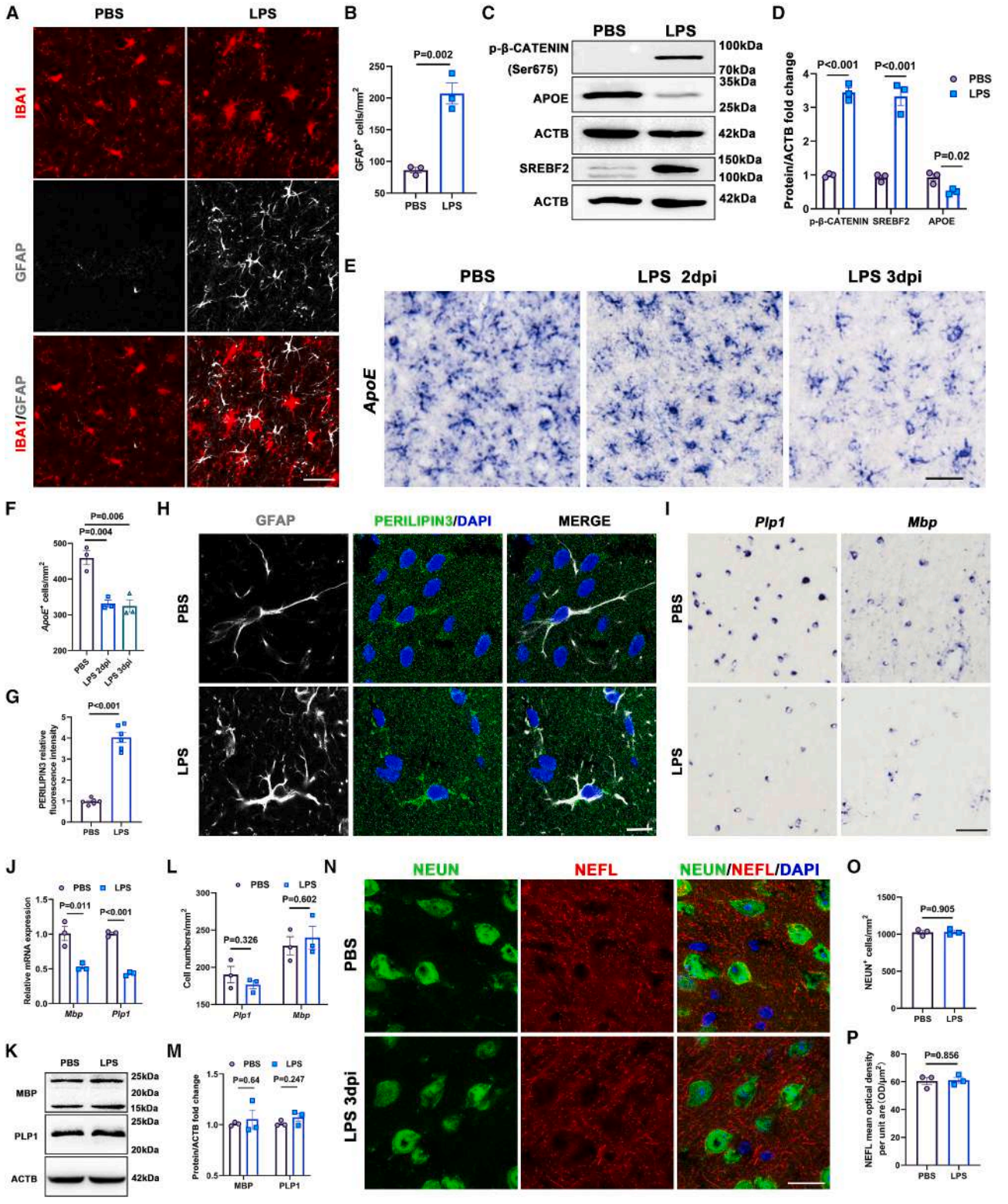


**Figure 1. Inflammatory responses activate Wnt signaling pathway in astrocytes, leading to cholesterol accumulation and downregulation of myelin gene expression**

(A and B) Immunofluorescent staining of microglial marker IBA1 (red) and astrocyte marker GFAP (white) was performed in the motor cortex of control and LPS-treated mice. The number of GFAP$^+$ cells was quantified. *n* = 3 mice. Scale bars, 50 μm.

*(legend continued on next page)*

expression of *ApoE*, which mediates cholesterol efflux. The diminished cholesterol supply decreases the expression of MYRF transcription factor and myelin-associated genes in oligodendrocytes, compromising myelin maintenance and integrity. This study identifies Wnt signaling as a key driver of a regulatory pathway of "neuroinflammation → Wnt signaling → astrocyte cholesterol metabolism → myelin integrity," providing a molecular target for therapeutic treatment of inflammation-related neurological disorders.

## RESULTS

### Inflammation induces Wnt signaling activation and cholesterol accumulation in astrocytes but impairs myelin gene expression in oligodendrocytes

To investigate the effects of inflammation on glial functions, we injected LPS into the lateral ventricle of adult mouse brain. LPS has been widely used to induce neuroinflammation in brain tissues.[17,18] Three days after LPS treatment, brain tissues were processed for immunohistochemical staining, which showed a marked increase in the number of activated GFAP-positive astrocytes and IBA1-positive microglia with an amoeboid activated morphology, confirming the effective induction of inflammation (Figures 1A and 1B). In line with the previous observations that Wnt/β-CATENIN pathway is frequently activated in inflammatory microenvironments,[15,16] cortical level of phospho-β-CATENIN (S675), a marker for Wnt pathway activation, was indeed elevated significantly (Figures 1C and 1D). In addition, we examined the effects of LPS-induced neuroinflammation on cholesterol synthesis and export and discovered that expression of sterol regulatory element-binding transcription factor 2 (SREBF2), a key transcriptional regulator of cholesterol biosynthesis, was also upregulated substantially (Figures 1C and 1D). Unexpectedly, expression of APOE, a major lipid- and cholesterol-transporting apolipoprotein, in cortical astrocytes declined dramatically at both the protein and transcriptional levels following LPS injection (Figures 1C–1F). Together, these results strongly suggest that inflammation suppresses the transcription of *ApoE* gene in astrocytes (Figures 1E and 1F). Consistent with this finding, PERILIPIN3 immunostaining revealed a large accumulation of lipid droplets in LPS-treated cortical astrocytes compared with the control cells (Figures 1G and 1H).

Considering that astrocytes are the primary source of cholesterol in the adult brain[19] and myelinating oligodendrocytes largely depend on the uptake of astrocyte-secreted cholesterol to maintain myelin turnover,[7] we next assessed the impact of neuroinflammation on myelin gene expression and structural integrity under inflammatory conditions. RNA *in situ* hybridization and qPCR analysis showed a dramatic reduction in the transcription of myelin genes *Mbp* and *Plp1* in the cortical tissue of the treatment group (Figures 1I and 1J). However, the total number of positive cells and protein levels did not change significantly (Figures 1L and 1M), possibly due to the slow turnover of mature Oligodendrocytes (OLs) and myelin structures during the 3-day LPS treatment period. The inhibition of myelin gene transcription suggests that cholesterol supplied by astrocytes plays a critical role in myelin growth and maintenance. To exclude the possibility that the observed myelin changes are secondary to neuronal or axonal loss, we performed NEUN and NEFL immunostaining in the cortex of LPS-treated mice. The results showed no significant differences in the number and distribution of NEUN-positive neurons or in the density and morphology of NEFL-labeled axons between the LPS-treated and the control groups (Figures 1N–1P), indicating that LPS treatment did not cause overt loss of neurons and axons within the 3-day time window.

To directly verify that LPS activates the Wnt signaling cascade and reduces APOE gene expression in astrocytes, we purified and cultured astrocytes from the brain tissues of neonatal mice in the presence or absence of LPS compound. Consistent with the *in vivo* findings, we observed a marked upregulation of downstream target genes of the Wnt signaling pathway in astrocytes within the initial 6 h post-LPS treatment (Figure 2A), along with a gradual increase in the level of phosphorylated β-CATENIN (p-β-CATENIN) in a time-dependent manner (Figures 2B and 2C) and the induced nuclear translocation of β-CATENIN (Figure 2H). Notably, LPS treatment also significantly upregulated the expression of SREBF2 (Figures 2D and 2E) and markedly elevated intracellular cholesterol levels (Figure 2F). However, APOE expression in astrocytes was downregulated (Figures 2D and 2E) in association with increased levels of intracellular cholesterol as revealed by both Filipin and BODIPY-cholesterol staining (Figures 2G–2J). Collectively, these results demonstrate that inflammation-induced activation of the Wnt

(C and D) Western blot assay to detect the levels of phospho-β-CATENIN, SREBF2, and APOE in the cortical tissue of mice from the PBS control group and the LPS-treated group, with ACTB serving as the loading control. Quantitative analysis of protein expression levels was presented as fold changes, $n = 3$ mice.
(E and F) *In situ* hybridization (ISH) to detect the mRNA expression levels of *ApoE* in the mouse motor cortex from the control and LPS-treated groups at 2 days post-injection (2 dpi) and 3 dpi, and the number of *ApoE* $^+$ cells was quantified. Scale bars, 50 μm, $n = 3$ mice.
(G and H) Immunofluorescent staining was performed to detect the co-expression of the astrocyte marker GFAP (white) and lipid droplet marker PERILIPIN3 (green) in the motor cortex of PBS- and LPS-treated mice. Nuclei were stained with 4',6-diamidino-2-phenylindole (DAPI) (blue). The fluorescence intensity of intracellular lipid droplet signals was quantified. $n = 6$ mice. Scale bars, 20 μm.
(I and L) Detection of *Mbp* and *Plp1* mRNA levels by ISH in the motor cortex from the PBS- and LPS-treated groups. The number of *Mbp*$^+$ and *Plp*1$^+$ cells was counted and quantified per mm$^2$. $n = 3$ mice. Scale bars, 100 μm.
(J) qPCR analysis of *Mbp* and *Plp1* expression in the cortex at 3 days after stereotaxic injection of LPS into the brain, $n = 3$ mice.
(K–M) Western blot assay to detect the myelin proteins MBP and PLP1 in the mouse cortex from the control and the LPS-treated groups, with ACTB serving as the loading control. Quantitative analysis of protein expression levels was presented as fold changes, $n = 3$ mice.
(N-P) Immunofluorescence of mouse motor cortex at 3 days post LPS induction. Quantification of NEUN$^+$ (neuronal nuclei, green) cell counting per mm$^2$ (O) and NEFL (neurofilament light chain, red) signal density (P). $n = 3$ mice; scale bars, 50 μm.
Error bars indicate SEM. *p* values are labeled on the bar charts. Assays (B), (D), (G), (J), (L), (M), (O), and (P) were analyzed using two-tailed unpaired Student's *t* test. Assay (F) was analyzed using one-way ANOVA followed by Dunnett's multiple comparisons test.

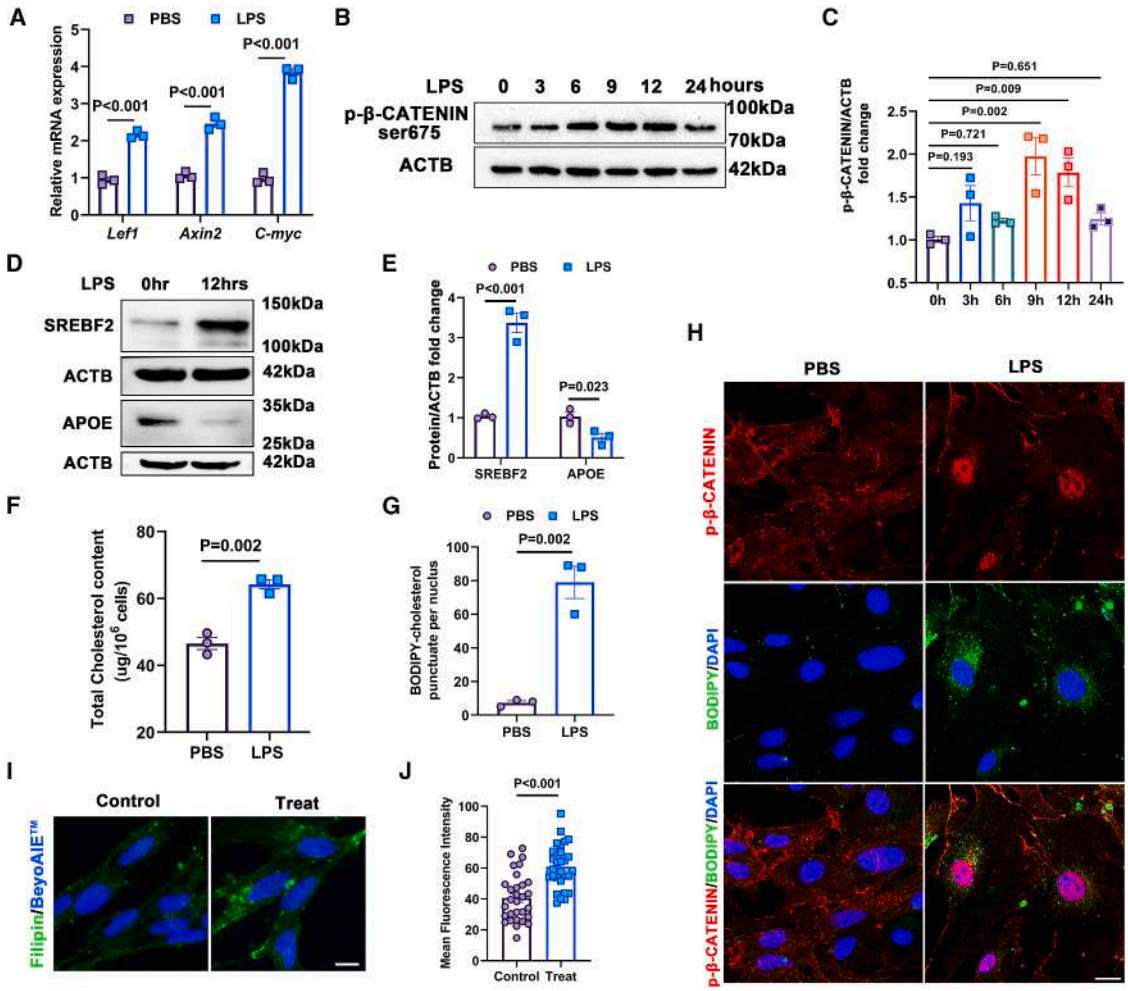


**Figure 2. LPS activates the Wnt signaling and induces cholesterol accumulation in astrocytes**

(A) qPCR analyses of the expression of Wnt signaling downstream genes after 6 h of LPS 1 μg/mL treatment. *n* = 3 independent experiments.

(B and C) Western blot assay to detect the phospho-β-CATENIN Ser675 levels in primary astrocytes treated with LPS 1 μg/mL for various time periods (0, 3, 6, 9, 12, and 24 h), with ACTB serving as the loading control. Quantitative analysis of protein expression levels was presented as fold changes, *n* = 3 independent experiments.

(D and E) Western blot assay to detect the SREBF2 and APOE protein expression in primary astrocytes after 12 h of LPS treatment, with ACTB serving as the loading control. Quantitative analysis of protein expression levels was presented as fold changes, *n* = 3 independent experiments.

(F) Determination of intracellular cholesterol content in primary astrocytes following 12 h of LPS treatment, *n* = 3 independent experiments.

(G and H) Immunofluorescent staining of primary astrocytes with phospho-β-CATENIN (Ser675) (red), BODIPY-cholesterol (green), and nuclei stained with DAPI (blue). Quantitative assessment of BODIPY-cholesterol is conducted around the periphery of the cell nucleus. *n* = 3 independent experiments, scale bars, 20 μm.

(I and J) Intracellular free cholesterol in primary astrocytes was stained with Filipin (green), and nuclei were counterstained with BeyoAIE (blue). Cells were divided into control and 12 h LPS-treated groups, and Filipin fluorescence intensity was quantified (*n* = 30 per group). Scale bars, 20 μm.

Error bars indicate SEM. *p* values are labeled on the bar charts. Assays (A), (E), (F), (G), and (J) were analyzed using two-tailed unpaired Student's *t* test. For assay (C), one-way ANOVA combined with Dunnett's multiple comparisons test was applied to compare each time point with the 0 h control group.

signaling pathway in astrocytes leads to aberrant intracellular cholesterol accumulation.

## Activation of Wnt signaling in astrocytes downregulates myelin gene expression in transgenic mice

To test the hypothesis that Wnt activation in astrocytes accounts for the diminished myelin gene expression in oligodendrocytes, we generated the *Aldh1l1-ER*$^{cre/+}$; *Ctnnb1-3Δex*$^{fx/+}$ inducible transgenic mouse model (hereinafter referred to as *Ctnnb1* GOF mice[20]) to delete exon 3 of the *Ctnnb1* gene (coding β-CATENIN) in astrocytes (Figure S1A). The removal of exon 3 prevents β-CATENIN protein from AXIN2 complex-mediated degradation and consequently increases its nuclear translocation and activation of the Wnt signaling pathway (Figure S1B).

To achieve the effective activation of the Wnt signaling pathway in astrocytes, we administered tamoxifen to 2-month-old adult mice for five consecutive days and then collected brain tissues two weeks later for histochemical analysis (Figure S1C).

As anticipated, qPCR analysis revealed a substantial upregulation of the expression of three well-known Wnt downstream target genes *Axin2*, *Lef1*, and *c-Myc* in the cortex (Figure S1D). Western blotting demonstrated a significantly elevated level of phosphorylated (activated) β-CATENIN (Figures S1E and S1F). Immunofluorescent staining showed the pronounced accumulation of β-CATENIN protein in the nuclei of GFAP-positive astrocytes (Figure S1G). Together, these results confirmed the successful establishment of the mouse model and the effective activation of the Wnt signaling cascade in cortical astrocytes.

Next, we investigated whether astrocytic activation of Wnt signaling can mimic the effects of LPS-induced inflammatory responses in transgenic tissues. Immunolabeling showed a remarkable surge in GFAP-positive cells in both the cortex and the striatum (Figures S2A–S2D), indicating the occurrence of reactive astrogliosis following Wnt pathway activation. However, we detected neither significant molecular and morphological alterations for microglia (Figures S2E and S2F) nor changes of c-Fos signal for neuronal activation (Figures S3A and S3B). Furthermore, NEUN and NEFL co-immunostaining revealed no significant differences between GOF and control mice in the number and distribution of NEUN-positive neurons or the density of NEFL-labeled axons (Figures S2G–S2I), arguing against the possibility that the observed myelin changes in GOF mice are secondary to neuronal damages. Thus, activation of the Wnt pathway in astrocytes had no apparent effects on the functioning of microglia and neurons during this two-week time window.

To analyze the effects of astrocytic Wnt activation on oligodendrocyte precursor cell (OPC) population dynamics, we assessed the proliferation and density of OPCs in GOF mice. The number of *Pdgfra*-positive OPCs was comparable between GOF and control mice (Figures S3C and S3D). Double immunostaining demonstrated that the proportion of $KI67^{+}SOX10^{+}$ proliferating OPCs did not differ significantly between groups (Figure S3E), indicating that OPC proliferation was not altered.

However, immunostaining for MYRF, a master transcription factor that marks newly formed oligodendrocytes (NFOs) and drives myelin gene expression, showed a dramatic reduction in the number of $MYRF^{+}$ cells in GOF cortical tissue (Figures 3A–3C). Immunolabeling showed that $ASPA^{+}$ mature oligodendrocytes were distributed normally in GOF mice, but the proportion of these cells that co-expressed MYRF was significantly diminished (Figures 3A–3C). Cell death assays showed no significant difference in the number of TUNEL-positive cells between GOF and control mice (Figure S3F), ruling out enhanced apoptosis as a cause of the diminished MYRF-expressing cell population.

Consistent with the reduced MYRF expression in OLs, the mRNA levels of *Plp1* and *Mbp* myelin genes declined substantially in GOF cortical tissue, indicating that myelin gene transcription in mature OLs was severely impaired in GOF brain tissue (Figures 3D–3H). However, expression of PLP1 and MOG were not significantly altered at the protein level in GOF mice (Figures S3G–S3I), indicating that myelinating oligodendrocytes and the pre-existing myelin sheaths were preserved during the two-week observation window. Consistently, TrueGold myelin staining showed that myelin fibers in GOF mice appeared moderately sparser than in controls (Figures 3I and 3J). Myelin ultrastructure, assessed by transmission electron microscopy (TEM), appeared to be normal and intact as myelin sheaths in GOF mice exhibited compact, regularly arranged lamellae, with no apparent signs of lamellar separation, vacuolization, or myelin ball formation. Quantitative g-ratio analysis revealed no significant difference between GOF and control mice (Figures 3K and 3L). Collectively, these findings suggest that the primary defect lies in the maintenance of myelin gene transcription in pre-existing differentiated oligodendrocytes, instead of the generation of new oligodendrocytes.

## Activation of Wnt signaling induces cholesterol accumulation in astrocytes

The downregulation of *ApoE* expression in cortical astrocytes of GOF mice strongly suggests that the cholesterol efflux from astrocytes to the extracellular space is obstructed, potentially leading to intracellular cholesterol accumulation. To test this idea, we biochemically measured intracellular total cholesterol levels in freshly isolated astrocytes via magnetic bead sorting and primary culture astrocytes and found that astrocytes from GOF mice exhibited significantly elevated levels of total cholesterol (Figure 4A). In parallel, we also found higher levels of free cholesterol staining by Filipin and lipid droplet staining by LipidSpot (Figures 4B–4E). More importantly, we discovered that cholesterol synthesis genes (*Srebf2* and *Hmgcr*) were upregulated, while efflux genes (*ApoE* and *Abca1*) were downregulated in freshly isolated astrocytes from GOF brain (Figure 4F). Meanwhile, expression of cholesterol uptake receptor gene *Ldlr* showed no significant difference from controls (Figure 4F). Together, these observations demonstrate that the cholesterol accumulation in GOF astrocytes primarily results from enhanced endogenous synthesis coupled with impaired efflux rather than increased uptake from the extracellular environment.

Based on these and other observations, we hypothesize that in GOF mice, cholesterol cannot be exported to the extracellular space, thereby preventing oligodendrocytes from acquiring sufficient exogenous cholesterol, which may enhance the transcription of myelin genes. To test this hypothesis, we purified OPCs and astrocytes from GOF mice and their control littermates. Astrocytes were first labeled with the BODIPY-cholesterol probe for 24 h, then co-cultured with OPCs for another 12 h before the transfer of cholesterol between these two cell types was assessed (Figure 4G). As hypothesized, the signal intensity of the BODIPY-cholesterol staining in oligodendrocytes co-cultured with GOF astrocytes was substantially lower than that with wild-type astrocytes (Figure 4H). Strikingly, the expression levels of the MYRF transcription factor and myelin genes MBP and PLP1 were markedly reduced (Figures 4I–4K), indicating that cholesterol transfer is essential for the differentiation of OPCs in the co-culture system lacking PDGF-AA mitogen.

## Wnt signaling regulates the transcription of genes controlling cholesterol synthesis and efflux

The cholesterol accumulation in astrocytes observed in the LPS-induced model is associated with abnormal expression of regulatory genes involved in cholesterol synthesis and transport (Figure 1). To investigate whether this aberrant gene expression is directly attributed to Wnt signaling activation, we examined the expression of *Srebf2* and *Hmgcr,* two regulatory genes that

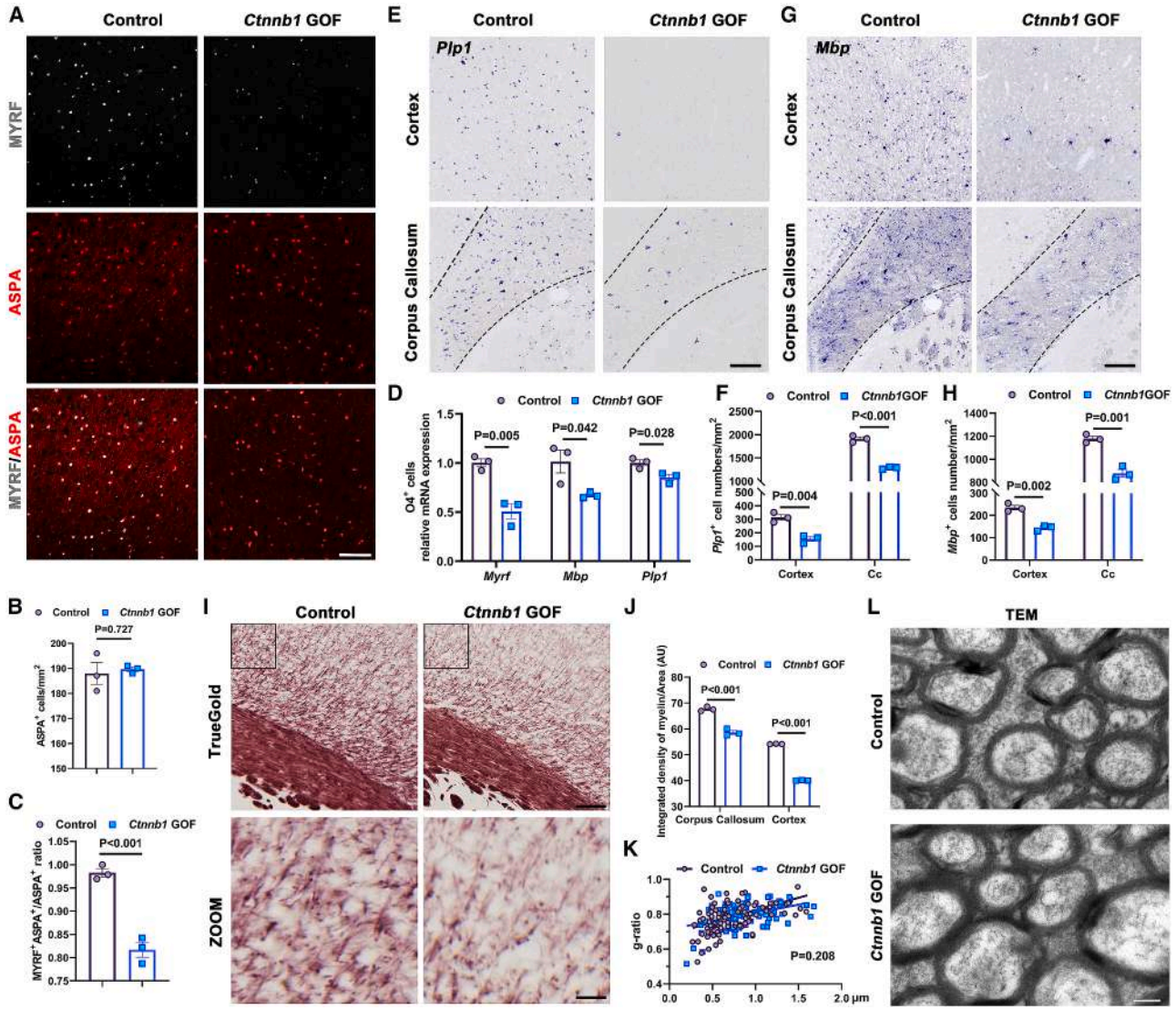


**Figure 3. Activation of Wnt signaling in astrocytes downregulates myelin gene expression**

(A–C) Immunofluorescence of MYRF (white) and ASPA (red) in mouse cortex. Statistics of ASPA$^+$ cells per mm$^2$ (B) and the ratio of MYRF$^+$/ASPA$^+$ double-positive cells to ASPA$^+$ cells (C) $n$ = 3. Scale bars, 100 μm.

(D) O4$^+$ oligodendrocytes sorted via Magnetically Activated Cell Sorting (MACS) from tamoxifen-treated adult mice were subjected to qPCR to quantify the mRNA levels of *Myrf*, *Mbp*, and *Plp1*. $n$ = 3 mice.

(E and F) RNA *in situ* hybridization (ISH) with *Plp1* probe in the motor cortex and corpus callosum of control and Ctnnb1 GOF mice. Statistical analysis of *Plp1*$^+$ cell numbers per mm$^2$. Scale bars, 100 μm; $n$ = 3 mice.

(G and H) ISH staining with *Mbp* probe in the motor cortex and corpus callosum of control and Ctnnb1 GOF mice. Statistical analysis of *Mbp*$^+$ cell numbers per mm$^2$. Scale bars, 100 μm; $n$ = 3 mice.

(I and J) TrueGold staining of brain tissues from control and *Ctnnb1* GOF mice. Quantitative analysis of myelin fiber density. Scale bars, 100 μm. The scale bars of the zoomed-in image represent 20 μm; $n$ = 3 mice.

(K and L) TEM images and g ratio analysis of myelinated axons in the corpus callosum. Scale bars, 0.2 μm.

Error bars indicate SEM. $p$ values are labeled on the bar charts. a.u., arbitrary units. $n$ = 3 mice. Assays (B), (C), (D), (F), (H), (J), and (K) were analyzed using two-tailed unpaired Student's $t$ test.

encode rate limiting enzymes in cholesterol biosynthesis pathway in GOF mouse model. As expected, the expression levels of these two genes increased substantially in both the cortical tissue and primary astrocytes derived from the GOF mice (Figures 5A–5C). Concurrently, the expression of *Acat1*, a gene regulating cholesterol esterification and promoting lipid droplet formation, also elevated significantly in GOF astrocytes (Figure 5A), coupled with the formation of numerous intracellular lipid droplets (Figure 4E). In contrast, expression of *ApoE* was downregulated profoundly at both the mRNA and protein levels

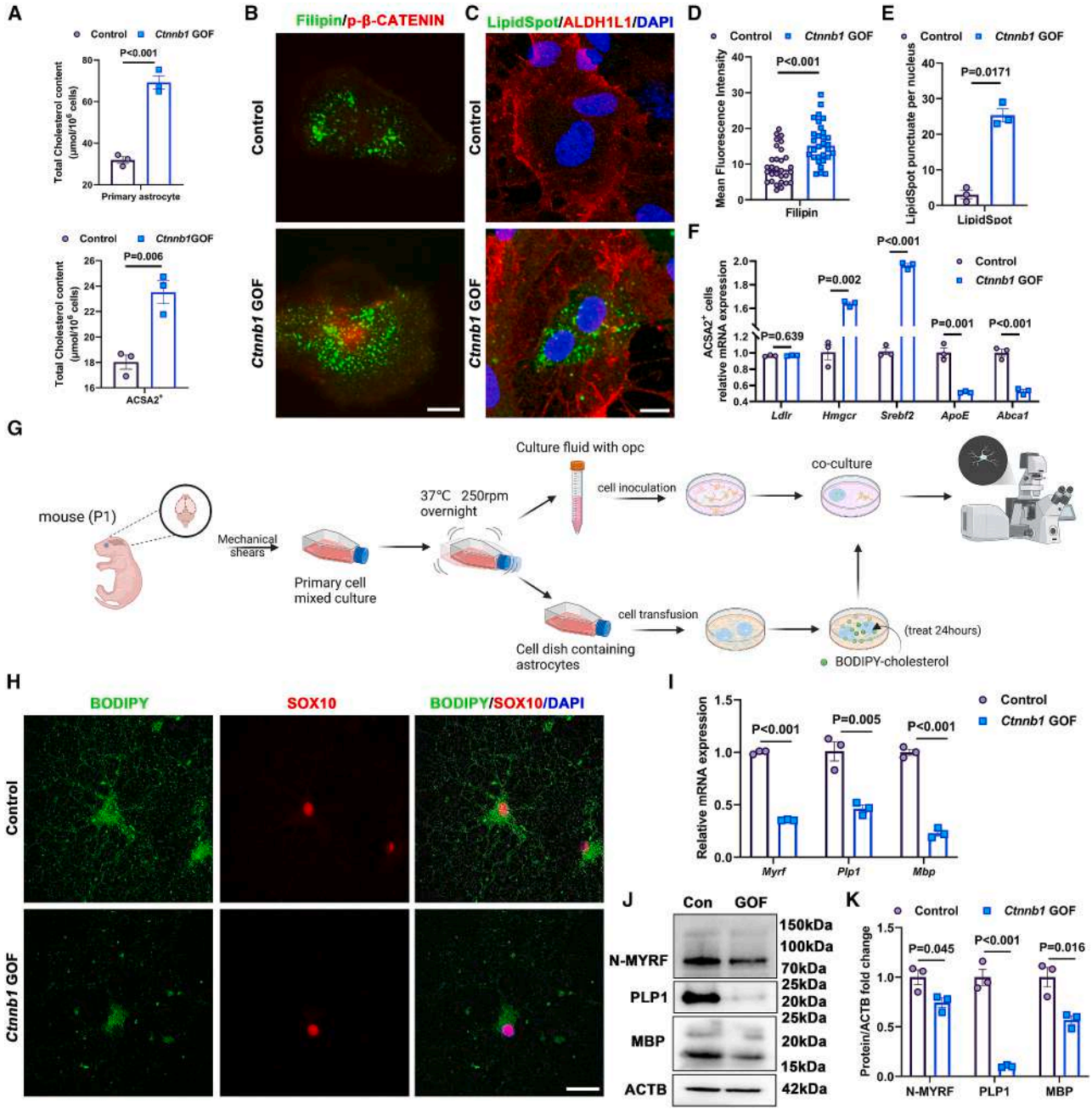


**Figure 4. Accumulation of cholesterol in astrocytes reduces cholesterol acquisition and myelin gene expression by oligodendrocytes**

(A) Intracellular cholesterol was detected in primary cortical astrocytes from P0 Control and *Ctnnb1* GOF mice after 7-day 4-OHT induction. ACSA2$^+$ astrocytes from tamoxifen-treated adult Control and *Ctnnb1* GOF mice were sorted by MACS for cholesterol analysis. *n* = 3 independent experiments.

(B–D) Immunofluorescence labeling of intracellular Filipin (green) and p-β-CATENIN Ser675(red) in primary astrocytes from control and *Ctnnb1* GOF mice. Quantitative analysis of Filipin signals. *n* = 30 per group. Scale bars, 20 μm.

(C–E) Immunofluorescent co-staining of lipid droplets (LipidSpot staining, green) and astrocyte marker ALDH1L1 (red) in primary astrocytes from control and *Ctnnb1* GOF mice. Quantitative assessment of LipidSpot is conducted around the periphery of the ALDH1L1$^+$ cell nucleus. Nuclei were stained with DAPI (blue). *n* = 3 independent experiments. Scale bars, 20 μm.

(F) ACSA2$^+$ astrocytes sorted by MACS from tamoxifen-treated adult mice were subjected to qPCR to analyze mRNA expression of *Ldlr*, *Hmgcr*, *Srebf2*, *ApoE*, and *Abca1*. *n* = 3 independent experiments.

(G) Experimental design for co-culture of primary astrocytes and oligodendrocytes from control and *Ctnnb1* GOF mice.

*(legend continued on next page)*

(Figures 5A–5C, 6A, and 6B), in parallel with the declined expression of another lipid transporter protein *Abca1* (Figure 5A). These results strongly suggest that activation of the Wnt signaling pathway in astrocytes differentially affects the expression of genes involved in cholesterol synthesis and transport.

Given that nuclear β-CATENIN can bind to transcription factors LEF1 and TCF7[21] and that *Srebf2* mRNA expression is increased in GOF astrocytes, we postulated that β-CATENIN is directly involved in *Srebf2* transcriptional regulation via LEF1/TCF7. Using JASPAR prediction, we identified one potential LEF1/TCF7 binding site in the mouse *Srebf2* promoter region, located between −664 and −814 bp upstream of the translation start site (Figure 5D), and in accordance, constructed a pGL3-basic-*Srebf2* expression vector for the dual-luciferase reporter assay. Co-transfection of this construct together with *Ctnnb1* and *Lef1* expression vectors in HEK293T cells demonstrated that overexpression of *Lef1* or *Ctnnb1* alone was able to raise *Srebf2* transcriptional activity (Figure 5E), but simultaneous expression of both further augmented this activity. When the LEF1 binding sites in the *Srebf2* promoter were point mutated, co-expression of *Ctnnb1* and *Lef1* failed to enhance the luciferase activity (Figure 5E). To further interrogate the regulatory relationship between β-CATENIN and *Srebf2*, we performed chromatin immunoprecipitation-PCR (ChIP-PCR) assays with anti-β-CATENIN, which confirmed the binding of β-CATENIN to the *Srebf2* promoter region (Figure 5F). Together, these findings demonstrate that β-CATENIN acts together with LEF1/TCF7 on the *Srebf2* promoter to stimulate its gene transcription in astrocytes.

To test the hypothesis that the lessened expression of *ApoE* in astrocytes impairs cholesterol efflux, we administered TBTC (methyl 2-amino-6-(tert-butyl)-4,5,6,7-tetrahydrobenzo(*b*)thiophene-3-carboxylate), a small molecule known to upregulate APOE expression,[22] to mutant mice via intraperitoneal injection. Immunostaining confirmed that TBTC treatment significantly increased APOE expression in the brains of GOF mice (Figures 6C and 6D) and restored the expression of *ApoE* in the inflammatory mouse model injected with LPS (Figures S4A–S4C). Meanwhile, RNA *in situ* hybridization and immunofluorescence demonstrated the restored expression of myelin-related genes *Plp1* and MYRF transcription factor in the GOF brain tissue (Figures 6E–6I). However, given that TBTC is a potential activator of retinoid X receptor α (RXRα), which has an important role in myelin development,[22–24] we also tested the effects of TBTC on OPC differentiation and maturation. We did not observe a significant change in myelin gene expression at the concentrations used in this experiment, supporting the direct role of TBTC in affecting astrocytic APOE expression (Figures S4D and S4E). These findings were further validated at the cellular level by the finding that overexpression of *ApoE* in primary astrocytes attenuated BODIPY staining in mutant astrocytes to the level comparable to that in control cells (Figures 6J and 6K). Collectively, these results demonstrate that APOE deficiency is likely to be the direct cause of impaired cholesterol efflux in mutant mice.

## Cholesterol regulates myelin gene expression through MYRF transcription factor

To elucidate the mechanism by which cholesterol regulates the expression of myelin genes in oligodendrocytes, we added exogenous cholesterol to primary OPCs cultures. Cholesterol was delivered as a water-soluble methyl-β-cyclodextrin (MβCD)-cholesterol complex to overcome its inherent insolubility in aqueous culture medium.[25,26] This method has been widely used for efficient delivery of cholesterol to the plasma membrane, followed by non-vesicular transport into intracellular compartments.[27,28] Strikingly, cholesterol treatment markedly increased the percentages of MYRF$^+$ NFOs and MBP$^+$ mature OLs in parallel with a significant decrease in PDGFRA$^+$ OPCs (Figure S5). qPCR analyses also manifested the gradual upregulation of myelin-related genes (*Myrf*, *Mbp*, and *Plp1*) with treatment time (Figure 7A). This result was verified by the RNA-seq analysis of 12 h treatment sample (Figure 7B) and further substantiated at the protein level by western blot and MYRF immunostaining (Figures 7C–7F). In contrast, expression of early differentiation genes at COP (committed oligodendrocyte progenitors) stage, such as *Bcas1*, *Fyn*, and *Gpr17*, was attenuated (Figure 7B). Altogether, this "shift from early to late stages" directly demonstrates that cholesterol promotes OPC differentiation along the oligodendrocyte lineage rather than simply upregulating myelin transcripts in already-differentiated cells.

Gene Ontology (GO) enrichment analysis also unveiled a significant enrichment of molecular pathways related to myelin structure and cholesterol synthesis, among others (Figure 7G). Concurrently, cholesterol treatment potently repressed the expression of *Hmgcr* and *Sqle* (two key genes for *de novo* cholesterol synthesis) and the cholesterol uptake receptor gene *Ldlr* in oligodendrocytes (Figure 7H), possibly owing to a feedback inhibition of intrinsic cholesterol synthesis by exogenous cholesterol.

Previous studies demonstrated that MYRF transcription factor functions as a master regulatory gene for myelin formation and maintenance.[29] It is plausible that MYRF may be directly involved in the cholesterol-induced expression of myelin gene expression. In agreement with this concept, cholesterol-treatment significantly enhanced the number of MYRF$^+$ cells (Figure 7E). In further support, when *Myrf* expression was knocked down in OPC culture, cholesterol-induced myelin gene expression was substantially attenuated (Figure 7I), demonstrating the crucial role of *Myrf* in the cholesterol-mediated regulation of myelin genes. Notably, when *Myrf* and

(H) Double staining of intracellular BODIPY (green) and oligodendrocyte marker SOX10 (red) in oligodendrocytes after co-culture. Fluorescent images were converted to grayscale using ImageJ to clearly visualize the diffuse distribution of lipids in oligodendrocytes (OLs). Nuclei were stained with DAPI (blue). Scale bars, 20 μm; $n = 3$ independent experiments.

(I) qPCR analysis of *Myrf*, *Plp*1, and *Mbp* mRNA levels in oligodendrocytes from the co-culture system. $n = 3$ independent experiments.

(J and K) Western blot assay to detect the N-MYRF, PLP1, and MBP protein levels in oligodendrocytes from the co-culture system, with ACTB serving as the loading control. Quantitative analysis of protein expression levels was presented as fold changes, $n = 3$ independent experiments.

Error bars indicate SEM. *p* values are labeled on the bar charts. Assays (A, D, E, F, I, and K) were analyzed using two-tailed unpaired Student's *t* test.

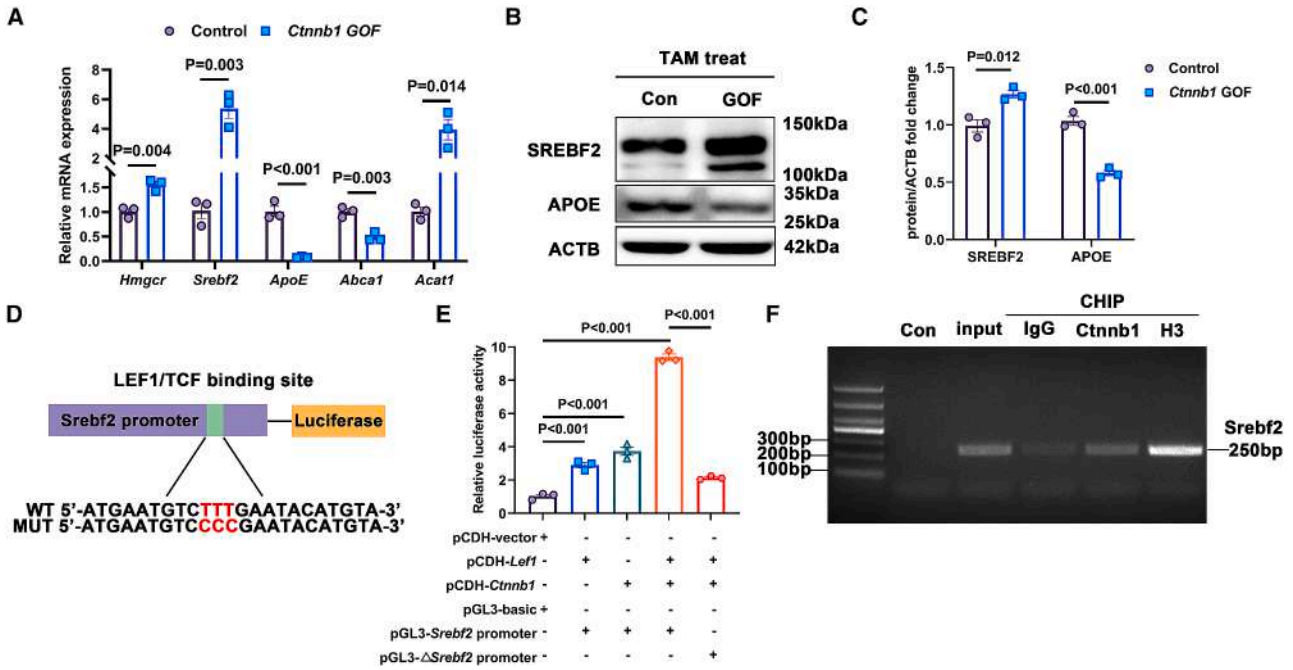


**Figure 5. Molecular mechanisms of Wnt signaling pathway in regulating cholesterol synthesis and transport**

(A) qPCR was performed to detect the mRNA levels of *Hmgcr*, *Srebf2*, *ApoE*, *Abca1*, and *Acat1* in primary astrocytes from control and *Ctnnb1* GOF mice following 4-OHT induction; $n = 3$ independent experiments.

(B and C) Western blot assay to detect the SREBF2 and APOE in primary mouse astrocytes, with ACTB serving as the loading control. Quantitative analysis of protein expression levels was presented as fold changes, $n = 3$ independent experiments.

(D) Schematic of the dual luciferase reporter construct placed under the *Srebf2* promoter region (upstream −1,300 to −1,920), depicting the LEF1/TCF binding sequence and the point mutation sites (red) in the mutant form (Mut).

(E) Double luciferase assays with various expression constructs as shown. The Fluc/Rluc ratio was calculated for each group, with the pRL-TK plasmid serving as the internal control, $n = 3$ independent experiments.

(F) ChIP-PCR analysis of the enrichment of the *Srebf2* promoter sequence in input and precipitated chromatin with IgG or anti-CTNNB1 antibody from mouse p7 brain.

Error bars indicate SEM. p values are labeled on the bar charts. Assays (A) and (C) were analyzed using two-tailed unpaired Student's *t* test. Assay (E) was analyzed using one-way ANOVA followed by Bonferroni's multiple comparisons test for pre-planned pairwise comparisons.

*Sox10* were knocked down simultaneously, cholesterol stimulation of myelin gene expression was further reduced to the level comparable to the untreated control cells (Figure 7I). One possible explanation for this result is that SOX10 is required for MYRF expression, and the induction of myelin genes by cholesterol relies on the synergistic action of MYRF and SOX10.

## DISCUSSION

### A novel signaling axis linking neuroinflammation to myelin integrity via astrocyte cholesterol metabolism

As a central hub for cholesterol metabolism in the CNS, the functional homeostasis of astrocytes is crucial for the development and maintenance of myelin.[8,30,31] This study reveals that under neuroinflammatory conditions, abnormal activation of the Wnt/β-CATENIN signaling pathway in astrocytes reshapes their cholesterol metabolism. While this metabolic reprogramming promotes cholesterol synthesis, it inhibits its efflux and causes aberrant intracellular cholesterol accumulation. This ultimately attenuates cholesterol supply to oligodendrocytes and impairs the expression of myelin genes. The present study identifies a signaling axis: "inflammation → Wnt/β-CATENIN signaling → astrocyte cholesterol anabolism → myelin integrity" (Figure 7J), providing a theoretical framework for understanding the pathological mechanisms of inflammation-related white matter injury and demyelinating diseases.

It should be emphasized that in this study, LPS was used to induce a complex neuroinflammatory environment, while the *Ctnnb1* GOF genetic model was specifically designed to isolate the astrocyte-autonomous effects of Wnt pathway activation in the absence of confounding inflammatory stimuli. The core phenotypes—SREBF2 upregulation, APOE downregulation, lipid droplet accumulation, and myelin gene suppression—are consistently reproduced across both models, strongly supporting that astrocytic Wnt signaling is a major contributor to the observed myelin pathology. Importantly, in the GOF model, microglial activation and neuronal c-Fos changes were not detected, and NEUN/NEFL immunostaining confirmed preserved neuronal and axonal integrity, demonstrating that these myelin-related changes are not secondary to broader neuroaxonal damage or microglia-mediated inflammation. The successful TBTC rescue in both GOF and LPS models further validates the

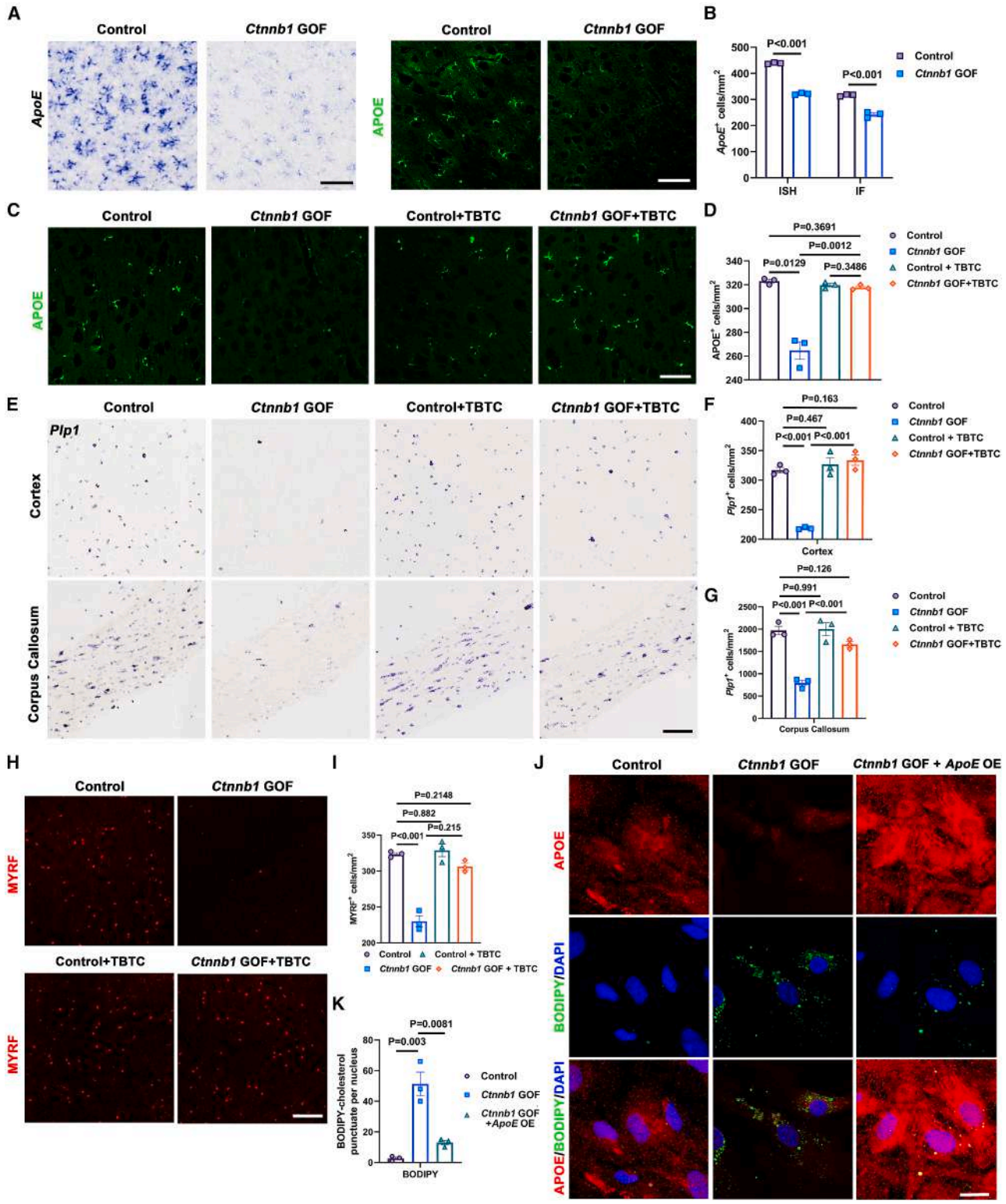


**Figure 6. Molecular mechanisms of Wnt signaling pathway in regulating cholesterol synthesis and transport**

(A and B) *In situ* hybridization with *ApoE* probe and immunofluorescent staining of APOE in cortical tissue from control and *Ctnnb1* GOF mice. Statistical assessment of *ApoE*$^+$ cells per mm$^2$; $n$ = 3 mice; scale bars, 50 μm.

*(legend continued on next page)*

therapeutic relevance of the proposed mechanism under inflammatory conditions and completes the logical chain from phenotype discovery to mechanism validation and therapeutic verification.

It should be noted, however, that the LPS-induced inflammatory milieu is complex and may activate multiple signaling pathways (e.g., NF-κB, STAT3, and MAPK) that could influence astrocytic cholesterol metabolism either synergistically or independently of Wnt signaling. While the GOF model shows that Wnt activation is sufficient to drive the observed metabolic and myelin phenotypes, it does not necessarily prove that Wnt signaling is necessary for these effects in the LPS model. Thus, our data suggest that Wnt signaling is a key driver, but not the sole mediator, of inflammation-induced remodeling of astrocyte cholesterol metabolism and myelin gene suppression.

### Bidirectional regulation of astrocyte cholesterol metabolism by Wnt signaling

One of the major findings in this study is that neuroinflammation specifically activates the canonical Wnt/β-CATENIN signaling pathway in astrocytes. Although Wnt signaling was suggested to be a key regulator of lipid metabolism in peripheral tissues (e.g., liver and adipose tissue),[12,13] its role in cholesterol metabolism within mature astrocytes has not been reported. Our data show that both LPS stimulation and conditional activation of β-CATENIN in astrocytes significantly upregulate the expression of the key cholesterol synthesis transcription factor *Srebf2* and its downstream genes (e.g., *Hmgcr*). Mechanistically, we found that the β-CATENIN/LEF/TCF7 transcriptional complex can directly bind to the *Srebf2* promoter region and drive its transcription. This finding suggests that Wnt signaling contributes to cellular metabolic regulation in the CNS and may act as a molecular switch connecting inflammation and metabolic reprogramming.

On the other hand, we found that activated Wnt/β-CATENIN signaling strongly suppresses the expression of *ApoE*, the major cholesterol-transporting apolipoprotein in astrocytes.[32–34] As a result, *ApoE* downregulation is associated with reduced delivery of cholesterol from astrocytes to oligodendrocytes. Conversely, in rescue experiments, TBTC compound induced APOE expression in astrocytes and effectively restored myelin gene expression both in GOF mice and in the LPS-induced inflammation model, confirming the central role of APOE in this pathway. However, several potential caveats should be considered for this rescue experiment. Firstly, given that TBTC is also a selective agonist of RXRα, which has been implicated in CNS myelination and lipid metabolism,[22–24] it remains plausible that certain rescue effects on myelin gene expression may involve RXRα-mediated pathways beyond *ApoE* upregulation. Secondly, as APOE is produced by multiple cell types in the CNS, including microglia, under inflammatory conditions, the TBTC-mediated APOE increase may not be exclusively astrocytic in origin. Thirdly, the reduced myelin gene expression in LPS model might not be caused by cholesterol deficiency per se; TBTC may also exert direct anti-inflammatory or pro-differentiation effects on oligodendrocytes. Therefore, additional experiments, such as astrocyte-specific *ApoE* overexpression or conditional knockout, are required to further prove that enhancing APOE-mediated cholesterol efflux in astrocytes is responsible for rescuing myelin gene expression.

The upregulation of SREBF2 and downregulation of APOE in activated astrocytes may be mediated through divergent mechanisms. While β-CATENIN/LEF1 directly activates *Srebf2* transcription, APOE suppression may involve inhibition of nuclear receptors such as LXR or the action of transcriptional repressors.[35] This bidirectional regulation, promoting synthesis while inhibiting efflux, results in intracellular cholesterol sequestration and lipid droplet formation. As this metabolic phenotype is observed in both LPS-induced inflammation and non-inflammatory GOF models, it may represent Wnt-driven metabolic reprogramming rather than non-specific astrocyte reactivity.

Previous work by Liddelow and colleagues demonstrated that reactive astrocytes activated by microglia-derived cytokines can secrete APOE-containing lipoparticles carrying long-chain saturated fatty acids, thereby driving neuronal and oligodendrocyte death.[36] In the context of Wnt-driven "pro-synthesis, anti-efflux" metabolic state, APOE downregulation in astrocytes may serve a protective function by limiting the secretion of lipoprotein particles that could potentially carry toxic saturated lipid species, while diverting excess cholesterol toward safe esterified storage in lipid droplets. Thus, our findings do not contradict but rather complement the Liddelow model, collectively highlighting the multidimensional metabolic plasticity of astrocytes under different inflammatory contexts.

As the primary supplier of cholesterol in the brain, the concurrent increase in synthesis and decrease in efflux may seem paradoxical. However, during early astrocyte development (e.g., E13.5 brain), Wnt signaling levels in precursor cells are significantly higher than in mature cells,[37] and the main tasks of astrocyte precursor cells are proliferation and migration,[38] requiring substantial lipids for membrane expansion. Cholesterol synthesized during this period is primarily for their own use, consistent

(C and D) APOE immunostaining (green) in control, *Ctnnb1* GOF, control + TBTC, and *Ctnnb1* GOF + TBTC groups. Statistical assessment of $APOE^+$ cells per $mm^2$; $n = 3$ mice, scale bars, 50 μm.

(E–G) *In situ* hybridization with *Plp1* probe in the motor cortex and corpus callosum of control group, *Ctnnb1* GOF group, control group injected with TBTC, and *Ctnnb1* GOF group injected with TBTC, with counting of positive cells per $mm^2$; $n = 3$ mice; scale bars, 100 μm.

(H and I) Immunofluorescence of MYRF (red) in the motor cortex of the control and *Ctnnb1* GOF groups in the absence or presence of TBTC treatment. Statistical assessment of $MYRF^+$ cells, $n = 3$ mice, scale bars, 100 μm.

(J and K) Primary astrocytes from control mice, *Ctnnb1* GOF mice, or from *Ctnnb1* GOF mice overexpressing exogenous *ApoE*. Cells were stained with immunofluorescent APOE (red), BODIPY (green), and nuclei with DAPI (blue). Quantitative assessment of BODIPY-cholesterol is conducted around the periphery of the $APOE^+$ cell nucleus. $n = 3$ independent experiments; scale bars, 20 μm.

Error bars indicate SEM. *p* values are labeled on the bar charts. Assay (B) was analyzed using two-tailed unpaired Student's *t* test. For assays (D), (F), (G), and (I), two-way ANOVA was applied to evaluate main effects and interaction, followed by Bonferroni's multiple comparisons test for pairwise comparisons. Assay (L) was analyzed using one-way ANOVA with Bonferroni's multiple comparisons for pairwise comparisons.

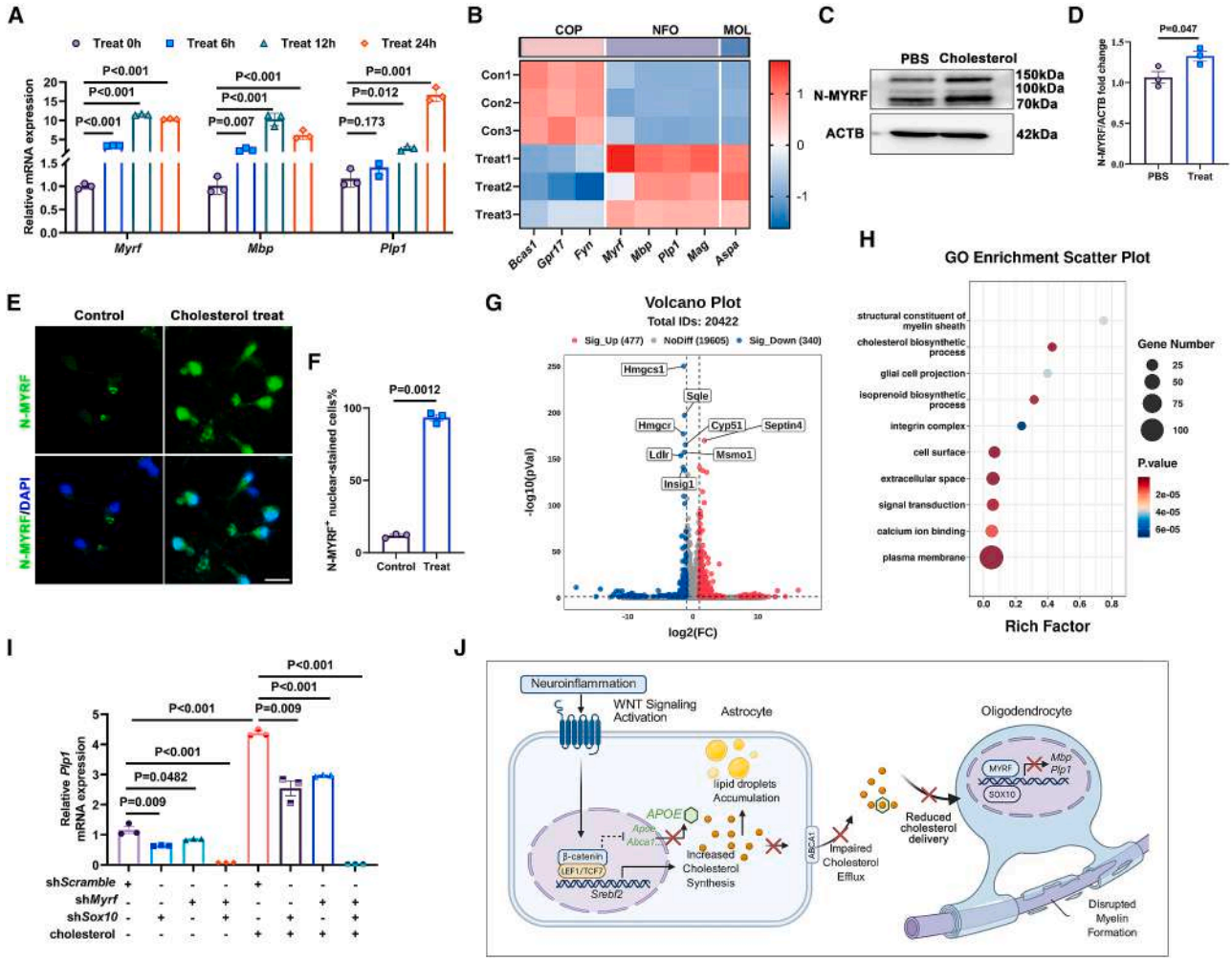


**Figure 7. Cholesterol regulates myelin gene expression through MYRF transcription factor**

(A) qPCR assays to detect the mRNA levels of *Myrf*, *Mbp*, and *Plp1* in primary oligodendrocytes after cholesterol treatment at 12 h; *n* = 3 independent experiments.

(B) RNA-seq heatmap shows altered mRNA expression of oligodendrocyte differentiation-related genes upon cholesterol treatment (*n* = 3 independent replicates). Red denotes upregulated gene expression; blue indicates downregulated transcription.

(C and D) Western blot assay to detect the protein level of MYRF in primary oligodendrocytes after cholesterol treatment. Quantitative analysis of protein expression levels was presented as fold changes, *n* = 3 independent experiments.

(E and F) Immunofluorescent staining of MYRF (green) in primary oligodendrocytes at 12 h after cholesterol addition, with statistical analysis of the nuclear translocation efficiency of MYRF; *n* = 3 independent experiments; scale bars, 20 μm.

(G) Peak plot of differentially expressed genes in primary oligodendrocytes after cholesterol addition. Red dot denotes upregulated gene; blue dot indicates downregulated gene.

(H) Gene Ontology (GO) enrichment analysis of primary oligodendrocytes after cholesterol addition, based on RNA-seq results.

(I) qPCR assay to detect the effect of cholesterol on *Plp1* expression after *Sox10* knockdown, *Myrf* knockdown, and simultaneous knockdown of both *Sox10* and *Myrf*, *n* = 3 independent experiments.

(J) A working model for neuroinflammation regulation of cholesterol homeostasis and myelin gene expression. Under inflammatory conditions, the Wnt signaling pathway is activated in astrocytes, leading to the nuclear translocation of the β-CATENIN/LEF/TCF complex. This complex binds to the promoter region of *Srebf2* and upregulates its expression, thereby enhancing the intracellular cholesterol synthesis pathway. In parallel, Wnt signaling represses the expression of *ApoE* and *Abca1* and consequently impedes cholesterol export out of astrocytes. Excess cholesterol accumulates intracellularly and forms lipid droplets. Oligodendrocytes fail to receive sufficient amount of cholesterol supplied by astrocytes, resulting in diminished expression of the transcription factor MYRF and its downstream target genes such as *Mbp* and *Plp*1, ultimately compromising myelin stability.

Error bars indicate SEM. *p* values are labeled on the bar charts. Assay (A) was analyzed using one-way ANOVA with Dunnett's multiple comparisons to compare each group with the control. Assays (D) and (F) were analyzed using two-tailed unpaired Student's *t* test. Two-way ANOVA combined with Bonferroni's multiple comparisons test was adopted for statistical analysis of assay (I).

with the relatively low level of *ApoE* expression. It is only during postnatal development that astrocytes in the mouse brain begin to upregulate *ApoE* expression, coinciding with their morphological and functional maturation.[39,40] Intriguingly, although Wnt signaling is activated in astrocyte precursor cells, it does not lead to cholesterol accumulation and lipid droplet formation. One possible explanation is that the level of Wnt signaling intensity is only moderate in astrocyte precursors, as compared with the significantly heightened activity under inflammatory or genetic mutation conditions.

## Cholesterol supply from astrocytes controls myelin gene expression through MYRF

A direct consequence of disrupted cholesterol metabolism in astrocytes is "cholesterol starvation" in oligodendrocytes. Using a co-culture system, we demonstrated that when Wnt pathway is activated, astrocytes transfer significantly less cholesterol to oligodendrocytes.

Mechanistic studies indicate that the cholesterol supply from astrocytes does not affect OPC proliferation or survival in GOF mice (Figures S3C–S3F) but exerts a profound effect on the function of core transcriptional network within oligodendrocytes for myelin production.[7] Exogenous cholesterol treatment significantly enhanced MYRF nuclear localization and the expression of a large number of downstream myelin genes. The pro-myelinating effect of cholesterol can be blocked by *Myrf* knockdown, in keeping with the previous studies establishing MYRF as the "master switch" for myelin gene expression.[29] However, given that MYRF protein accumulates during OPC differentiation, it remains plausible that cholesterol promotes oligodendrocyte differentiation through a distinct mechanism that, in turn, elevates MYRF levels. Nevertheless, the synergistic requirement of MYRF and SOX10 for cholesterol-stimulated myelin gene transcription establishes MYRF as a critical node in this regulatory axis. Moreover, SOX10 and MYRF exhibit a synergistic role in the cholesterol-enhanced myelin gene expression, which aligns with earlier findings indicating that *Sox10* regulates the expression of *Myrf*.[41,42] Quantitative analysis of stage-specific gene expression demonstrated that cholesterol promotes the NFO-associated gene expression. Considering that both *Myrf* mRNA and full-length MYRF protein are upregulated after cholesterol treatment, the most parsimonious explanation is that cholesterol promotes *Myrf* gene transcription or mRNA stability either directly or indirectly. Whether cholesterol also modulates MYRF cleavage or nuclear translocation at the posttranslational level remains an open and interesting question for future studies. Intriguingly, we also discovered that exogenous cholesterol strongly suppressed the expression of genes involved in intrinsic cholesterol synthesis (e.g., *Hmgcr* and *Sqle*) and cholesterol uptake (e.g., *Ldlr*) within oligodendrocytes, suggesting a feedback inhibition mechanism triggered by neighboring cells to maintain intracellular cholesterol homeostasis,[43] highlighting the highly coordinated nature of cholesterol supply from astrocytes to oligodendrocytes.

It is worth mentioning that in GOF mouse model, cholesterol primarily acts on differentiated oligodendrocytes to maintain myelin gene transcription and local myelin renewal. In culture system, OPCs possess strong differentiation potential and cholesterol functions to drive their differentiation and initiate myelin gene expression. Despite this discrepancy, the core molecular mechanism is consistent across both systems: cholesterol converges on MYRF to upregulate myelin-associated gene expression, as evidenced by the bidirectional validation of "reduced cholesterol supply → MYRF downregulation → myelin gene suppression" *in vivo* and "increased cholesterol supply → MYRF upregulation → myelin gene activation" *in vitro*.

## Pathophysiological relevance and pharmacological considerations

The "inflammation-Wnt-cholesterol-myelin" axis unveiled by this study holds significant pathophysiological relevance. Neuroinflammation is a common feature of various neurological disorders (e.g., multiple sclerosis, Alzheimer's disease, stroke, and brain injury) and is often accompanied by white matter damage.[44–46] Previous research has largely focused on the direct toxicity of inflammatory cytokines to oligodendrocytes or their inhibition of precursor cell differentiation.[47,48] Our work delineates a mechanistic pathway initiated by the metabolic dysfunction of supporting astrocytes. The inflammatory microenvironment first "hijacks" Wnt signaling in astrocytes, altering their metabolic phenotype. This may chronically impair myelin maintenance and repair by disrupting the long-term supportive function of cholesterol supply, which could explain why progressive white matter rarefaction and functional decline occurs in some chronic inflammatory or aging processes even in the absence of obvious acute demyelination.[49] Simultaneously, this study provides a perspective on the role of Wnt signaling in neurological diseases. While previous research primarily focused on its roles in development, tumorigenesis, or the blood-brain barrier,[21,50,51] our findings suggest that in the mature brain, neuroinflammation is associated with abnormal activation of the Wnt pathway in astrocytes, which may disrupt metabolic homeostasis and contribute to pathological processes.

## Limitations of the study

Several limitations of this study should be acknowledged. First, the present work primarily employed an acute LPS-induced inflammation model rather than disease-relevant chronic models such as Experimental Autoimmune Encephalomyelitis (EAE) or aging-related white matter injury. Whether the same molecular mechanisms operate under chronic inflammatory conditions and whether sustained transcriptional suppression eventually leads to myelin deterioration and functional deficits, requires further validation. Second, while our gain-of-function genetic approach demonstrates that Wnt activation in astrocytes is sufficient to recapitulate the core phenotypes, it does not establish that Wnt signaling is necessary for these effects in the LPS model. Complementary loss-of-function experiments would be required to firmly address causality. Third, our assessments of microglial and neuronal status were limited to morphological markers (IBA1, CD68, NEUN, and NEFL) and immediate-early gene expression (c-Fos); more comprehensive functional analyses, such as cytokine profiling or synaptic physiology, were not performed. Finally, although APOE is clearly implicated in cholesterol efflux, we cannot rule out the involvement of other

lipid transporters (e.g., ABC family members) or the integration of Wnt signaling with other inflammatory pathways (e.g., NF-κB and STAT3) in regulating this process.

## RESOURCE AVAILABILITY

### Lead contact

Requests for further information and resources should be directed to and will be fulfilled by the lead contact, Kang Zheng (zhengkang@hznu.edu.cn).

### Materials availability

This study did not generate new unique reagents.

### Data and code availability

- The raw data from this study were deposited in the NCBI Sequence Read Archive under accession number SRA: GSE324225.
- This paper does not report original code.
- Any additional information required to reanalyze the data reported in this paper is available from the lead contact upon request.

## ACKNOWLEDGMENTS

This work was supported by ST12030-Major Projects 2022ZD0204700 (China), National Natural Science Foundation of China (32170969 and 32371022), and Zhejiang Provincial Natural Science Foundation of China (LY22C090002).

## AUTHOR CONTRIBUTIONS

M.Q. and K.Z. conceived the study and designed the experiments; C.H., J. Zhao, M.Q., and K.Z. jointly supervised the study; J. Zhang, J. Zheng, and Y.A. performed the research; J. Zhang, J.Y., and K.Z. analyzed the data; J. Zhang, C.H., J. Zhao, M.Q., and K.Z. wrote and revised the manuscript. All authors edited and approved the final manuscript.

## DECLARATION OF INTERESTS

The authors declare no competing interests.

## STAR★METHODS

Detailed methods are provided in the online version of this paper and include the following:



## SUPPLEMENTAL INFORMATION

Supplementary data related to this article can be found online at https://doi.org/10.1016/j.celrep.2026.117871.

Received: March 6, 2026
Revised: July 7, 2026
Accepted: July 31, 2026

## REFERENCES

1. Wuerch, E.C., and Yong, V.W. (2025). Cholesterol in the CNS: functions, recycling and remyelination. J. Neuroinflammation *22*, 180. https://doi.org/10.1186/s12974-025-03490-8.
2. Griffiths, L., Hawkins, K., Yutuc, E., Angelini, R., Fosuah, R., Pacciarini, M., Dickson, A., Robertson, N., Childs, L., Loveless, S., et al. (2025). Sterol imbalances and cholesterol-24-hydroxylase dysregulation is linked to the underlying progression of multiple sclerosis. Brain Pathol. *35*, e70001. https://doi.org/10.1111/bpa.70001.
3. Zhao, Q., Li, J., Feng, J., Wang, X., Liu, Y., Wang, F., Liu, L., Jin, B., Lin, M., Wang, Y.C., et al. (2025). Cholesterol metabolic reprogramming mediates microglia-induced chronic neuroinflammation and hinders neurorestoration following stroke. Nat. Metab. *7*, 2099–2116. https://doi.org/10.1038/s42255-025-01379-7.
4. Barnes-Vélez, J.A., Aksoy Yasar, F.B., and Hu, J. (2023). Myelin lipid metabolism and its role in myelination and myelin maintenance. Innovation *4*, 100360. https://doi.org/10.1016/j.xinn.2022.100360.
5. Festa, L.K., Grinspan, J.B., and Jordan-Sciutto, K.L. (2024). White matter injury across neurodegenerative disease. Trends Neurosci. *47*, 47–57. https://doi.org/10.1016/j.tins.2023.11.003.
6. Osso, L.A., and Hughes, E.G. (2024). Dynamics of mature myelin. Nat. Neurosci. *27*, 1449–1461. https://doi.org/10.1038/s41593-024-01642-2.
7. Camargo, N., Goudriaan, A., van Deijk, A.L.F., Otte, W.M., Brouwers, J.F., Lodder, H., Gutmann, D.H., Nave, K.A., Dijkhuizen, R.M., Mansvelder, H.D., et al. (2017). Oligodendroglial myelination requires astrocyte-derived lipids. PLoS Biol. *15*, e1002605. https://doi.org/10.1371/journal.pbio.1002605.
8. Molina-Gonzalez, I., Holloway, R.K., Jiwaji, Z., Dando, O., Kent, S.A., Emelianova, K., Lloyd, A.F., Forbes, L.H., Mahmood, A., Skripuletz, T., et al. (2023). Astrocyte-oligodendrocyte interaction regulates central nervous system regeneration. Nat. Commun. *14*, 3372. https://doi.org/10.1038/s41467-023-39046-8.
9. Shrivastava, V., Tyagi, S., Dey, D., Singh, A., Palanichamy, J.K., Sinha, S., Sharma, J.B., Seth, P., and Sen, S. (2024). Glial cholesterol redistribution in hypoxic injury in vitro influences oligodendrocyte maturation and myelination. Biochim. Biophys. Acta. Mol. Basis Dis. *1870*, 167476. https://doi.org/10.1016/j.bbadis.2024.167476.
10. Pfrieger, F.W., and Ungerer, N. (2011). Cholesterol metabolism in neurons and astrocytes. Prog. Lipid Res. *50*, 357–371. https://doi.org/10.1016/j.plipres.2011.06.002.
11. Zhang, J., and Liu, Q. (2015). Cholesterol metabolism and homeostasis in the brain. Protein Cell *6*, 254–264. https://doi.org/10.1007/s13238-014-0131-3.
12. Sharma, A., Zalejski, J., Bendre, S.V., Kavrokova, S., Hasdemir, H.S., Ozgulbas, D.G., Sun, J., Pathmasiri, K.C., Shi, R., Aloulou, A., et al. (2025). Cholesterol-targeting Wnt-β-catenin signaling inhibitors for colorectal cancer. Nat. Chem. Biol. *21*, 1376–1386. https://doi.org/10.1038/s41589-025-01870-y.
13. Behari, J., Yeh, T.H., Krauland, L., Otruba, W., Cieply, B., Hauth, B., Apte, U., Wu, T., Evans, R., and Monga, S.P.S. (2010). Liver-specific beta-catenin

knockout mice exhibit defective bile acid and cholesterol homeostasis and increased susceptibility to diet-induced steatohepatitis. Am. J. Pathol. *176*, 744–753. https://doi.org/10.2353/ajpath.2010.090667.

14. Ye, H., Liu, Q., Wang, Y., Zhen, X., and Yan, N. (2023). The Effect of Cholesterol Efflux on Endothelial Dysfunction Caused by Oxidative Stress. Int. J. Mol. Sci. *24*, 5939. https://doi.org/10.3390/ijms24065939.

15. Vallée, A. (2022). Neuroinflammation in Schizophrenia: The Key Role of the WNT/β-Catenin Pathway. Int. J. Mol. Sci. *23*, 2810. https://doi.org/10.3390/ijms23052810.

16. Ji, R.R., Xu, Z.Z., and Gao, Y.J. (2014). Emerging targets in neuroinflammation-driven chronic pain. Nat. Rev. Drug Discov. *13*, 533–548. https://doi.org/10.1038/nrd4334.

17. Skrzypczak-Wiercioch, A., and Sałat, K. (2022). Lipopolysaccharide-Induced Model of Neuroinflammation: Mechanisms of Action, Research Application and Future Directions for Its Use. Molecules *27*, 5481. https://doi.org/10.3390/molecules27175481.

18. Zhang, X., Tian, X., Wang, Y., Yan, Y., Wang, Y., Su, M., Lv, H., Li, K., Hao, X., Xing, X., and Song, S. (2024). Application of lipopolysaccharide in establishing inflammatory models. Int. J. Biol. Macromol. *279*, 135371. https://doi.org/10.1016/j.ijbiomac.2024.135371.

19. Gao, Y., Ye, S., Tang, Y., Tong, W., and Sun, S. (2023). Brain cholesterol homeostasis and its association with neurodegenerative diseases. Neurochem. Int. *171*, 105635. https://doi.org/10.1016/j.neuint.2023.105635.

20. Harada, N., Tamai, Y., Ishikawa, T., Sauer, B., Takaku, K., Oshima, M., and Taketo, M.M. (1999). Intestinal polyposis in mice with a dominant stable mutation of the beta-catenin gene. EMBO J. *18*, 5931–5942. https://doi.org/10.1093/emboj/18.21.5931.

21. Nusse, R., and Clevers, H. (2017). Wnt/β-Catenin Signaling, Disease, and Emerging Therapeutic Modalities. Cell *169*, 985–999. https://doi.org/10.1016/j.cell.2017.05.016.

22. Sun, Y., Fan, J., Zhu, Z., Guo, X., Zhou, T., Duan, W., and Shen, X. (2015). Small molecule TBTC as a new selective retinoid X receptor α agonist improves behavioral deficit in Alzheimer's disease model mice. Eur. J. Pharmacol. *762*, 202–213. https://doi.org/10.1016/j.ejphar.2015.05.050.

23. Natrajan, M.S., de la Fuente, A.G., Crawford, A.H., Linehan, E., Nuñez, V., Johnson, K.R., Wu, T., Fitzgerald, D.C., Ricote, M., Bielekova, B., and Franklin, R.J.M. (2015). Retinoid X receptor activation reverses age-related deficiencies in myelin debris phagocytosis and remyelination. Brain *138*, 3581–3597. https://doi.org/10.1093/brain/awv289.

24. Zhou, X., He, C., Ren, J., Dai, C., Stevens, S.R., Wang, Q., Zamler, D., Shingu, T., Yuan, L., Chandregowda, C.R., et al. (2020). Mature myelin maintenance requires Qki to coactivate PPARβ-RXRα-mediated lipid metabolism. J. Clin. Investig. *130*, 2220–2236. https://doi.org/10.1172/jci131800.

25. Christian, A.E., Haynes, M.P., Phillips, M.C., and Rothblat, G.H. (1997). Use of cyclodextrins for manipulating cellular cholesterol content. J. Lipid Res. *38*, 2264–2272.

26. Härtel, S., Diehl, H.A., and Ojeda, F. (1998). Methyl-beta-cyclodextrins and liposomes as water-soluble carriers for cholesterol incorporation into membranes and its evaluation by a microenzymatic fluorescence assay and membrane fluidity-sensitive dyes. Anal. Biochem. *258*, 277–284. https://doi.org/10.1006/abio.1998.2594.

27. Ikonen, E., and Olkkonen, V.M. (2023). Intracellular Cholesterol Trafficking. Cold Spring Harbor Perspect. Biol. *15*, a041404. https://doi.org/10.1101/cshperspect.a041404.

28. Ferrari, A., and Tontonoz, P. (2025). Nonvesicular cholesterol transport in physiology. J. Clin. Investig. *135*, e188127. https://doi.org/10.1172/jci188127.

29. Huang, H., Zhou, F., Zhou, S., and Qiu, M. (2021). MYRF: A Mysterious Membrane-Bound Transcription Factor Involved in Myelin Development and Human Diseases. Neurosci. Bull. *37*, 881–884. https://doi.org/10.1007/s12264-021-00678-9.

30. Saher, G., and Stumpf, S.K. (2015). Cholesterol in myelin biogenesis and hypomyelinating disorders. Biochim. Biophys. Acta *1851*, 1083–1094. https://doi.org/10.1016/j.bbalip.2015.02.010.

31. Werkman, I.L., Kövilein, J., de Jonge, J.C., and Baron, W. (2021). Impairing committed cholesterol biosynthesis in white matter astrocytes, but not grey matter astrocytes, enhances in vitro myelination. J. Neurochem. *156*, 624–641. https://doi.org/10.1111/jnc.15113.

32. Rawat, V., Wang, S., Sima, J., Bar, R., Liraz, O., Gundimeda, U., Parekh, T., Chan, J., Johansson, J.O., Tang, C., et al. (2019). ApoE4 Alters ABCA1 Membrane Trafficking in Astrocytes. J. Neurosci. *39*, 9611–9622. https://doi.org/10.1523/jneurosci.1400-19.2019.

33. Michikawa, M., Fan, Q.W., Isobe, I., and Yanagisawa, K. (2000). Apolipoprotein E exhibits isoform-specific promotion of lipid efflux from astrocytes and neurons in culture. J. Neurochem. *74*, 1008–1016. https://doi.org/10.1046/j.1471-4159.2000.0741008.x.

34. Li, X., Zhang, J., Li, D., He, C., He, K., Xue, T., Wan, L., Zhang, C., and Liu, Q. (2021). Astrocytic ApoE reprograms neuronal cholesterol metabolism and histone-acetylation-mediated memory. Neuron *109*, 957–970.e8. https://doi.org/10.1016/j.neuron.2021.01.005.

35. Makoukji, J., Shackleford, G., Meffre, D., Grenier, J., Liere, P., Lobaccaro, J.M.A., Schumacher, M., and Massaad, C. (2011). Interplay between LXR and Wnt/β-catenin signaling in the negative regulation of peripheral myelin genes by oxysterols. J. Neurosci. *31*, 9620–9629. https://doi.org/10.1523/jneurosci.0761-11.2011.

36. Guttenplan, K.A., Weigel, M.K., Prakash, P., Wijewardhane, P.R., Hasel, P., Rufen-Blanchette, U., Münch, A.E., Blum, J.A., Fine, J., Neal, M.C., et al. (2021). Neurotoxic reactive astrocytes induce cell death via saturated lipids. Nature *599*, 102–107. https://doi.org/10.1038/s41586-021-03960-y.

37. Szewczyk, L.M., Lipiec, M.A., Liszewska, E., Meyza, K., Urban-Ciecko, J., Kondrakiewicz, L., Goncerzewicz, A., Rafalko, K., Krawczyk, T.G., Bogaj, K., et al. (2024). Astrocytic β-catenin signaling via TCF7L2 regulates synapse development and social behavior. Mol. Psychiatr. *29*, 57–73. https://doi.org/10.1038/s41380-023-02281-y.

38. Selvaraj, P., Xiao, L., Lee, C., Murthy, S.R.K., Cawley, N.X., Lane, M., Merchenthaler, I., Ahn, S., and Loh, Y.P. (2017). Neurotrophic Factor-α1: A Key Wnt-β-Catenin Dependent Anti-Proliferation Factor and ERK-Sox9 Activated Inducer of Embryonic Neural Stem Cell Differentiation to Astrocytes in Neurodevelopment. Stem Cell. *35*, 557–571. https://doi.org/10.1002/stem.2511.

39. Mouchel, Y., Lefrançois, T., Fages, C., and Tardy, M. (1995). Apolipoprotein E gene expression in astrocytes: developmental pattern and regulation. Neuroreport *7*, 205–208.

40. Stoll, G., and Müller, H.W. (1986). Macrophages in the peripheral nervous system and astroglia in the central nervous system of rat commonly express apolipoprotein E during development but differ in their response to injury. Neurosci. Lett. *72*, 233–238. https://doi.org/10.1016/0304-3940(86)90519-7.

41. Hornig, J., Fröb, F., Vogl, M.R., Hermans-Borgmeyer, I., Tamm, E.R., and Wegner, M. (2013). The transcription factors Sox10 and Myrf define an essential regulatory network module in differentiating oligodendrocytes. PLoS Genet. *9*, e1003907. https://doi.org/10.1371/journal.pgen.1003907.

42. Emery, B. (2013). Playing the field: Sox10 recruits different partners to drive central and peripheral myelination. PLoS Genet. *9*, e1003918. https://doi.org/10.1371/journal.pgen.1003918.

43. Luo, J., Yang, H., and Song, B.L. (2020). Mechanisms and regulation of cholesterol homeostasis. Nat. Rev. Mol. Cell Biol. *21*, 225–245. https://doi.org/10.1038/s41580-019-0190-7.

44. Wang, Q., Huang, X., Su, Y., Yin, G., Wang, S., Yu, B., Li, H., Qi, J., Chen, H., Zeng, W., et al. (2022). Activation of Wnt/β-catenin pathway mitigates blood-brain barrier dysfunction in Alzheimer's disease. Brain *145*, 4474–4488. https://doi.org/10.1093/brain/awac236.

45. Huang, Y.L., Zhang, J.N., Hou, T.Z., Gu, L., Yang, H.M., and Zhang, H. (2022). Inhibition of Wnt/β-catenin signaling attenuates axonal

degeneration in models of Parkinson's disease. Neurochem. Int. *159*, 105389. https://doi.org/10.1016/j.neuint.2022.105389.

46. Marchetti, B., Tirolo, C., L'Episcopo, F., Caniglia, S., Testa, N., Smith, J.A., Pluchino, S., and Serapide, M.F. (2020). Parkinson's disease, aging and adult neurogenesis: Wnt/β-catenin signalling as the key to unlock the mystery of endogenous brain repair. Aging Cell *19*, e13101. https://doi.org/10.1111/acel.13101.

47. Xiao, Y., and Czopka, T. (2023). Myelination-independent functions of oligodendrocyte precursor cells in health and disease. Nat. Neurosci. *26*, 1663–1669. https://doi.org/10.1038/s41593-023-01423-3.

48. Pan, R., Zhang, Q., Anthony, S.M., Zhou, Y., Zou, X., Cassell, M., and Perlman, S. (2020). Oligodendrocytes that survive acute coronavirus infection induce prolonged inflammatory responses in the CNS. Proc. Natl. Acad. Sci. USA *117*, 15902–15910. https://doi.org/10.1073/pnas.2003432117.

49. Seixas, A.I., Azevedo, M.M., Paes de Faria, J., Fernandes, D., Mendes Pinto, I., and Relvas, J.B. (2019). Evolvability of the actin cytoskeleton in oligodendrocytes during central nervous system development and aging. Cell. Mol. Life Sci. *76*, 1–11. https://doi.org/10.1007/s00018-018-2915-8.

50. Langen, U.H., Ayloo, S., and Gu, C. (2019). Development and Cell Biology of the Blood-Brain Barrier. Annu. Rev. Cell Dev. Biol. *35*, 591–613. https://doi.org/10.1146/annurev-cellbio-100617-062608.

51. Zhang, K., Zhang, J., Han, L., Pu, P., and Kang, C. (2012). Wnt/beta-catenin signaling in glioma. J. Neuroimmune Pharmacol. *7*, 740–749. https://doi.org/10.1007/s11481-012-9359-y.

52. Jiang, C., Hu, Y., Zhang, F., Qiu, M., and Zhao, X. (2026). Hippocampal Oligodendrocytes Regulate Mossy Fiber Development Involved in Epileptic Responses. Neurosci. Bull. *42*, 781–794. https://doi.org/10.1007/s12264-025-01452-x.

53. Dai, Z.M., Guo, W., Yu, D., Zhu, X.J., Sun, S., Huang, H., Jiang, M., Xie, B., Zhang, Z., and Qiu, M. (2022). SECISBP2L-Mediated Selenoprotein Synthesis Is Essential for Autonomous Regulation of Oligodendrocyte Differentiation. J. Neurosci. *42*, 5860–5869. https://doi.org/10.1523/jneurosci.2141-21.2022.

54. Xu, X., Fang, M., Chen, L., Huang, H., Dai, Z.M., Yang, J., and Qiu, M. (2024). Nzf2 promotes oligodendrocyte differentiation and regeneration via repressing HDAC1-mediated histone deacetylation. Sci. Adv. *10*, eadf8405. https://doi.org/10.1126/sciadv.adf8405.

## STAR★METHODS

### KEY RESOURCES TABLE

| REAGENT or RESOURCE | SOURCE | IDENTIFIER |
|---|---|---|
| Antibodies | | |
| anti-SOX10 | Oasis Biofarm | Cat# OB-PGP001; RRID: AB_2934230 |
| anti-MYRF | Oasis Biofarm | Cat# OB-PRB007; RRID: AB_2934255 |
| anti-PLP1 | Oasis Biofarm | Cat# OB-PRB071; RRID: AB_2938821 |
| anti-GFAP | Oasis Biofarm | Cat# OB-PGP055; RRID: AB_2938933 |
| anti-PDGFRA | Oasis Biofarm | Cat# OB-PRB011; RRID: AB_2938683 |
| anti-C FOS | Oasis Biofarm | Cat# OB-PGP055; RRID: AB_2938933 |
| anti-NEUN | Oasis Biofarm | Cat# OB-PRB039; RRID: AB_2934232 |
| anti-IBA1 | Oasis Biofarm | Cat# OB-MRT012; RRID: AB_3677303 |
| anti-ASPA | Oasis Biofarm | Cat# OB-PRT005; RRID: AB_2938679 |
| anti-NEFL | Oasis Biofarm | Cat# OB-PRT059; RRID: AB_2938903 |
| anti-MOG | Oasis Biofarm | Cat# OB-PRB134-; RRID: AB_2943407 |
| anti-KI67 | Oasis Biofarm | Cat# OB-PGP124; RRID: AB_3699168 |
| anti-SREBF2 | HUABIO | Cat# ER60160 |
| anti-CD68 | Oasis Biofarm | Cat# OB-PRB044; RRID: AB_2938840 |
| anti-ALDH1L1 | Oasis Biofarm | Cat# OB-PRB001; RRID: AB_2934257 |
| anti-APOE | Oasis Biofarm | Cat# OB-PRT028; RRID: AB_2938959 |
| anti-MBP | Oasis Biofarm | Cat# OB-PRT123; RRID: AB_3608272 |
| anti-Phospho-Beta Catenin (Ser675) | Proteintech | Cat# 80084-1-RR; RRID: AB_2918863 |
| anti-PERILIPIN3 | Proteintech | Cat# 66523-1-Ig; RRID: AB_2881886 |
| anti-ACTB | HUABIO | Cat# HA610019 |
| Goat anti-Mouse IgG1,488 | Invitrogen | Cat# A-21121; RRID: AB_2535764 |
| Goat-*anti*-Rabbit IgG(H + L), 594 nm | Invitrogen | Cat# A11012; RRID: AB_2534079 |
| Goat-*anti*-Rabbit IgG(H + L), 488 nm | Invitrogen | Cat# A11006; RRID: AB_2534074 |
| Goat-*anti*-Rat IgG(H + L), 488 nm | Oasis Biofarm | Cat# G-RT488 |
| Goat-*anti*-Rat IgG(H + L), 594 nm | Oasis Biofarm | Cat# G-RT594 |
| Goat-*anti*-Guinea pig IgG(H + L) 594 nm | Invitrogen | Cat# A11076; RRID: AB_2534120 |
| Goat-*anti*-Guinea pig IgG(H + L), 488 nm | Invitrogen | Cat# A11073; RRID: AB_2534117 |
| Goat-*anti*-Guinea pig IgG(H + L), 647nm | Invitrogen | Cat# A-21450; RRID: AB_2535867 |
| Goat-*anti*-Mouse IgG(H + L) HRP | Invitrogen | Cat#31430; RRID: AB_228307 |
| Goat-*anti*-Rabbit IgG(H + L) HRP | Invitrogen | Cat# 31460; RRID: AB_228341 |
| Goat-*anti*-Rat IgG(H + L) HRP | Invitrogen | Cat# 31470; RRID: AB_228356 |
| Bacterial and virus strains | | |
| *Myrf*-shRNA virus | This paper | N/A |
| *Sox10*-shRNA virus | This paper | N/A |
| *ApoE*-overexpression virus | This paper | N/A |
| Chemicals, peptides, and recombinant proteins | | |
| 0.25% trypsin-EDTA | Beyotime | Cat# GNM25200-1 |
| Fetal Bovine Serum | Excell | Cat# FSP500 |
| DMEM/F12 | Gibco | Cat# C11330500BT |
| Poly-L-lysine (PLL) | Merck | Cat# P7886 |
| Pasteur pipette | BIOFIL | Cat# PP205050 |
| Tamoxifen | Sigma | Cat# T5648 |
| 4-OH Tamoxifen | Sangon | Cat# A420345-0010 |

(*Continued on next page*)

*Continued*

| REAGENT or RESOURCE | SOURCE | IDENTIFIER |
|---|---|---|
| DMEM | Gibco | Cat# C11995500BT |
| Penicillin-streptomycin | Cellmax | Cat# CPS101.02 |
| N2 | Gibco | Cat# 17502048 |
| B27 | Gibco | Cat# 17504044 |
| PDGF-AA | novoprotein | Cat# CH74 |
| Water-soluble cholesterol | Sigma | Cat# C4951 |
| Mowiol | Sigma | Cat# 81381 |
| BODIPY-Cholesterol (488) | Sigma | Cat# 878557-19-8 |
| LipidSpot | Biotium | Cat# 70065 |
| Filipin | Beyotime | Cat# C2061 |
| BeyoAIE$^{TM}$ | Beyotime | Cat# C2105S |
| Trizol | TAKARA | Cat# 9108 |
| paraformaldehyde | Sigma | Cat# P6148 |
| Antigen retrieval solution | Sangon | Cat# E673001 |
| Goat serum | Gibco | Cat# 16210072 |
| T4 DNA polymerase | Beyotime | Cat# D7008 |
| TBTC | MCE | Cat# HY-121671 |
| LPS | Solarbio | Cat# L8880 |
| **Critical commercial assays** | | |
| Gold Myelin Stain Solution | Oasis Biofarm | Cat# BK-AC001 |
| Cholesterol Content Detection Kit | Sangon | Cat# D799800-0100 |
| Dual Luciferase Reporter System Kit | Promega | Cat# E1910 |
| Reverse Transcription Kit | Vazyme | Cat# R312-02 |
| qPCR Kit | Vazyme | Cat# P222-02 |
| DAB | Vector Laboratories | Cat# SK-4100 |
| SimpleChIP® Enzymatic Chromatin IP Kit (Magnetic Beads) | Cell Signaling Technology | Cat# 9003 |
| ECL Chemiluminescence Reagent | Fdbio | Cat# FD8000 |
| TUNEL kit | Roche | Cat# 11684795910 |
| Mycoplasma PCR Detection Kit | Beyotime | Cat# C0301S |
| **Deposited data** | | |
| Raw and analyzed data | This paper | GEO: GSE324225 |
| **Experimental models: Cell lines** | | |
| Primary astrocyte | Mouse (This paper) | P0-P1 |
| Primary OPCs | Mouse/Rat (This paper) | P0-P1 |
| HEK 293 T | ATCC | Cat# CVCL_0063 |
| ACSA2$^{+}$ cells | Mouse (This paper) | Adult |
| O4$^{+}$ cells | Mouse (This paper) | Adult |
| **Experimental models: Organisms/strains** | | |
| *Ctnnb1* GOF mouse | The Jackson Laboratory (JAX, discontinued strain); maintained in our laboratory | N/A |
| Wild-type C57BL/6 J mouse | N/A | N/A |
| Aldh1L1-ER$^{cre/+}$ mouse | Jackson Laboratory | Cat# 031008 |
| **Oligonucleotides** | | |
| All primer sequences | This paper | Table S1 |
| **Recombinant DNA** | | |
| pGL3-Basic | Promega | Cat# E1741 |
| pCDH-CMV-MCS-EF1-copGFP | System Biosciences | Cat# CD521A-1 |

(*Continued on next page*)

*Continued*

| REAGENT or RESOURCE | SOURCE | IDENTIFIER |
|---|---|---|
| pRL-TK | Promega | Cat# E2241 |
| pGreenPuro™ shRNA | SBI | Cat# SI505A-1 |
| psPax2 | Addgene | Cat# 12260 |
| pMD2.G | Addgene | Cat# 12259 |
| pCDH-CMV-MCS-Lef1-EF1-copGFP | This paper | N/A |
| pCDH-CMV-MCS-Ctnnb1-EF1-copGFP | This paper | N/A |
| pCDH-CMV-MCS-ApoE-EF1 | This paper | N/A |
| pGL3-Srebf2-Basic | This paper | N/A |
| pGL3-Srebf2(Mut)-Basic | This paper | N/A |
| GreenPuro™ shRNA-Myrf | This paper | N/A |
| GreenPuro™ shRNA-Sox10 | This paper | N/A |
| Software and algorithms | | |
| GraphPad Prism Ver. 8.4 | GraphPad Software | https://www.graphpad.com/features |
| ZEN 2 (blue edition) | Zeiss | https://www.zeiss.com/microscopy/us/products/software/zeiss-zen.html |
| LAS X | Leica | https://cn.leica-microsystems.com.cn/service/software-download |
| ImageJ | ImageJ | https://imagej.net/Downloads |
| Microsoft Excel | Microsoft | https://www.microsoft.com/en-us/microsoft-365/excel |
| Biorender | Biorender | https://www.biorender.com |
| PrimePCR™ Analysis Software | Biorad | https://www.bio-rad.com/zh-cn/product/primepcr-pcr-primers-assays-arrays?ID=M0HROA15#fragment-6 |

## EXPERIMENTAL MODEL AND STUDY PARTICIPANT DETAILS

### Animals

Animal husbandry and experiments were approved by the Animal Care and Use Committee of Hangzhou Normal University (approval number: HSD-20260729-01). *Ctnnb1-3Δex*$^{fx/+}$,[20] and *Aldh1l1-ER*$^{cre/+}$ mouse (JAX, 031008) were purchased from Jackson Laboratory (Bar Harbor, ME, USA). *Aldh1l1-ER*$^{cre/+}$ mice were crossed with *Ctnnb1-3Δex*$^{fx/+}$ mice to generate gain-of-function *Aldh1l1-ER*$^{cre/+}$; *Ctnnb1-3Δex*$^{fx/+}$ mice (*Ctnnb1* GOF). All mice were bred and maintained on a C57BL/6 background. Experimental analyses did not distinguish between male and female mice. All animals were group-housed at a 12 h light-dark cycle (light on from 8 a.m. to 8 p.m.) with food and water available *ad libitum*. Animals were randomly assigned to different experimental groups.

### Cell culture

P0-P1 neonatal mice were decapitated after disinfection with 75% ethanol, and brains were placed in pre-chilled sterile PBS(Biosharp, BL302A). Under dissecting microscope, remove meninges and blood vessels to isolate the cerebral cortex, then shear into tissue chunks approximately 1 $mm^3$. Discard PBS, add 0.25% trypsin-EDTA (Beyotime, GNM25200-1), and digest at 37°C water bath for 5 min, repeating digestion multiple times. Terminate digestion each time by adding serum-containing medium. Fetal bovine serum (FBS) was obtained from Excell (FSP500). Cell culture medium was DMEM/F12 (Gibco, C11330500BT). Repeat pipetting tissue chunks with a Pasteur pipette (BIOFIL, PP205050) until a single-cell suspension form. Centrifuge at 1000 rpm for 5 min and discard the supernatant. Resuspend the cell pellet in complete medium, adjusting the cell density to $1 \times 10^6$–$2\times10^6$ cells/mL. Seed the cells onto PLL (Poly-L-Lysine, Merck, P7886)-coated culture dishes (BIOFIL, TCF011250) and incubate at 37°C in a 5% $CO_2$ incubator. Change medium every 3 days. After 7 days of culture, when cell confluence exceeds 95%, perform purification by shaking: Place culture flasks on a 37°C constant-temperature shaker at 200 rpm for 1 h to remove microglia. Then shake at 250 rpm for 18–24 h. The supernatant yields oligodendrocyte precursor cells (OPCs). After centrifuging the supernatant, it is placed in a PLL-free culture dish (Sangon, F611003) for 1 h to allow non-OPC cells to adhere. Following this, the medium containing OPCs is aspirated, centrifuged, resuspended, and plated to obtain purified OPCs. Primary OPC cells were plated onto PLL-coated glass coverslips at a density of 10,000 cells/$cm^2$ using DMEM/F12 supplemented with N2 (Gibco, 17502048), B27 (Gibco, 17504044), and PDGF-AA (20 ng/mL, Novoprotein, CH74).

Primary astrocytes were routinely cultured in Dulbecco's modified Eagle's medium (DMEM, Gibco, C11995500BT) supplemented with 20% fetal bovine serum and penicillin-streptomycin (1000 U/mL; Cellmax, CPS101.02) in a humidified incubator with 5% $CO_2$ at

37°C, while adherent cells represent high-purity astrocytes, for primary GOF mouse astrocytes, induction requires the addition of 1 μM 4-OH TAM(Sangon, A420345-0010) to the culture medium for at least 5 days.

HEK293T cells (American Type Culture Collection (ATCC), RRID: CVCL_0045) were routinely cultured in Dulbecco's modified Eagle's medium (DMEM) (CellMax, CGM102.05) supplemented with 10% fetal bovine serum (FBS) (Biological Industries, 04-001-01 A) and penicillin-streptomycin (1000 U/mL; Gibco, 15140148) in a humidified incubator with 5% $CO_2$ at 37°C. The HEK293T cell line was authenticated via STR DNA profiling. Mycoplasma contamination was examined using a commercial Mycoplasma PCR Detection Kit, and the result confirmed the absence of mycoplasma.

## METHOD DETAILS

### Tamoxifen induction and tissue harvest of mouse

Genomic DNA was extracted from tails of embryonic or adult mice for subsequent genotyping via PCR. Genotyping PCR utilized primers described on the Jackson Laboratory website (https://www.jax.org/cn/). Tamoxifen (Sigma-Aldrich, T5648) was dissolved in corn oil at a concentration of 20 mg/mL and administered at a dose of 75 mg/kg for five consecutive days. Mice were anesthetized by intraperitoneal injection of pentobarbital sodium. After thoracotomy, perfusion was performed via left ventricular puncture: pre-perfuse with pre-cooled PBS to flush out circulating blood until the liver and limbs turned pale, followed by fixation with 4% paraformaldehyde (PFA). After whole-body stiffening, the brain was dissected rapidly and post-fixed in 4% PFA overnight at 4°C. Subsequently, tissues were dehydrated in gradient sucrose solution for frozen section preparation.

### Co-culture

Astrocytes and oligodendrocyte precursor cells (OPCs) were isolated from GOF mice via the above-described protocol. After induction with 4-hydroxytamoxifen, astrocytes were labeled with BODIPY-cholesterol for 24 h and then co-cultured with purified OPCs for 12 h. OPC culture medium depleted of PDGF-AA was applied during co-culture, and fluorescence signals were detected in the two cell types afterward.

### Cholesterol treatment of primary oligodendrocytes

Prepare a stock solution of water-soluble cholesterol (methyl-β-cyclodextrin (MβCD)–cholesterol complex, Sigma, C4951) using ultrapure water. Induce primary oligodendrocytes with a final concentration of 10 μM and collect cells at different time points. For shRNA-infected primary OPCs, cells were cultured for 2 days following lentiviral transduction, then treated with 10 μM water-soluble cholesterol for 12 h before sample collection for subsequent qPCR detection. For the OPC differentiation assay in Figure S5, primary rat OPCs were treated with 5 μM water-soluble cholesterol and continuously cultured for 3 days prior to immunofluorescence detection. The 10 μM cholesterol concentration was not adopted here since prolonged incubation at this dosage for two days induced obvious OPCs death due to excessive cholesterol concentration.

### Magnetic bead sorting

Remove whole brains from control and *Ctnnb1* GOF mice into PBS (Biosharp)-filled culture dishes to remove blood and meninges. Using ophthalmic forceps, cut cortical tissue into $1mm^3$ microtissues in medium dishes. Add digestion buffer (3 mL), digest for 5 min at 37°C in an incubator, decant supernatant, and terminate digestion by adding complete medium. Repeat digestion of tissue chunks 5 times, collecting each supernatant. Centrifuge supernatants, resuspend in magnetic bead sorting buffer, and load onto the column (Miltenyi, 130-042-201, 130-096-670). Follow the manufacturer's protocol for column loading (Miltenyi, Anti-ACSA-MB Kit, Anti-O4-MB Kit). Digestive buffer: Papain (0.1%) + DNase 25 (0.1%) + PBS. Magnetic bead sorting buffer: 2 mM EDTA +0.5% BSA + PBS pH 7.2.

### TrueGold staining

TrueGold staining was performed according to a previous method.[52] 14 μm frozen sections were washed three times in $ddH_2O$. TrueGold myelin staining solution (Oasis Biofarm, BK-AC001) was added to the tissue sections and incubated at 45°C in the dark until signal development. After adding stop solution for 2 min, rinse with $ddH_2O$, cover with Mowiol (Sigma, 81381) mounting medium, and photograph using a Leica microscope (DM6B).

### Transmission electron microscopy

For transmission electron microscopy, corpus callosum tissues were initially fixed in 2.5% glutaraldehyde solution for 4 h, followed by post-fixation with 1% osmium tetroxide (prepared in 0.1 M phosphate buffer, pH 7.0) at room temperature for 2 h. Samples were subsequently dehydrated through a graded ethanol series (50%, 70%, 80%, 90%, 95% and 100%) and pure acetone, with each step incubated for 20 min at ambient temperature. Specimens were embedded in Epon 812 resin and polymerized at 60°C to form solid resin blocks. Ultrathin sections with a thickness of 70 nm were cut using a diamond knife on a Leica UC 6 ultramicrotome. After double staining with uranyl acetate and lead citrate for 15 min, the sections were examined under an H-7650 transmission electron microscope.

### Cholesterol content assay in cells and cortex

Cholesterol content was measured using a kit (Sangon Biotech, D799800-0100) following the manufacturer's protocol.

### BODIPY-cholesterol, LipidSpot and filipin staining

BODIPY-cholesterol (Sigma, 878557-19-8) was added to the culture medium. Cells were incubated for 30 min in a cell culture incubator, washed three times with PBS, fixed with 4% PFA (Sigma, P6148), and proceeded to immunofluorescence experiments. LipidSpot (Biotium, 70065) staining was performed similarly. Filipin staining was conducted after secondary antibody incubation of immunofluorescence. Filipin working solution was prepared according to the manufacturer's protocol (Beyotime, C2061). Coverslips were incubated with the staining solution at room temperature in darkness for 90 min and washed three times with PBS, followed by incubation with BeyoAIE (Beyotime, C2105S). After additional PBS rinses, slides were mounted. Pseudocolors were adjusted during imaging, with filipin presented in green and BeyoAIE in blue. Images were captured using a Zeiss LSM710 confocal microscope, followed by z stack 3D reconstruction.

### Dual-luciferase assay

Prior to detecting dual-luciferase activity, the translation initiation sequence from mouse *Srebf2* was cloned into the pGL3-Basic vector (Promega, E1741) using T4 DNA polymerase (Beyotime, D7008). *Lef1* (GenBank: NM_001276403.1) and *Ctnnb1* (GenBank: NM_001165902.2) were cloned into the pCDH-CMV-MCS-EF1-copGFP (pCDH) vector (System Biosciences, CD521A-1). Transfection of HEK293T cells was performed in groups according to experimental requirements using 1 μg of pGL3-basic/pGL3-*Srebf2*-WT/pGL3-*Srebf2*-Mut, 200 ng of pRL-TK (Promega, E2241) plasmid, and 200 ng of pCDH-vector, pCDH-*Lef1*, and pCDH-*Ctnnb1*. Luciferase activity was measured using a dual-luciferase reporter system (Promega, E1910).

### TBTC injection and LPS treatment

TBTC was purchased from MCE (HY-121671). Injected at 30 mg/kg according to the manufacturer's recommended concentration.[22] For *Ctnnb1* GOF mice, consecutive intraperitoneal TBTC administration was performed for 7 days starting at day 5 post-tamoxifen induction. In LPS-challenged mice, TBTC was injected daily for 3 successive days beginning on the day of LPS treatment. For *in vitro* culture, LPS (Solarbio, L8880) was used at 1 μg/mL for astrocytes, and primary oligodendrocyte precursor cells were treated with LPS at the identical concentration for 12 h. For *in vivo* stereotaxic injection, 2 μL LPS solution (2.5 μg/μL) was delivered into the unilateral lateral ventricle, and mice in the control group received an equivalent volume of PBS.

### shRNA construction, virus production, and cell infection

The vector used is the pGreenPuro shRNA Cloning and Expression Lentivector (SBI, SI505A-1). The shRNA fragment sequences are listed in Table S1. The shRNA fragments were obtained using the method provided in the vector manual, then ligated into the vector using T4 ligase. The vector was transformed into *E*. coli, positive clones were screened, and plasmids were extracted. Efficiency was verified after cell transfection. For lentivirus preparation, co-transfected HEK293T cells with shRNA empty vector, shRNA expression vector, psPax2 (Addgene, 12260), and pMD2.G (Addgene, 12259) at a 4:3:1 mass ratio. Collect virus-containing medium at 24, 48, and 72 h post-transfection, filter through a 0.45 μm membrane (Millipore, SLHV033RB) to produce high-titer lentivirus.[53] Similarly, astrocyte infection with *ApoE*-overexpressing (*ApoE*-OE) plasmid was also achieved via the lentiviral system.

### RNA sequencing

RNA extraction, cDNA synthesis, library preparation, and sequencing were performed by Lianchuan Bio. Transcriptome libraries were prepared from 1 μg of total RNA using the TruSeq RNA Sample Preparation Kit (Illumina, USA). Sequencing was performed on an Illumina NovaSeq 6000 sequencer. To identify differentially expressed genes (DEGs) in oligodendrocytes following cholesterol treatment, gene expression levels were calculated using the FPKM method, with *Z* score transformations applied during plotting based on FPKM expression values. Differential expression analysis was conducted using DESeq2. Differentially expressed genes with log2FC > 1 and p-adj <0.05 were considered significantly differentially expressed. Gene Ontology (GO) analysis was performed using Goatools (http://github.com/tanghaibao/Goatools) to identify differentially expressed genes significantly enriched in GO terms relative to the whole transcriptome background.

### ChIP-PCR

Chromatin immunoprecipitation (ChIP) assays were performed with the SimpleChIP Enzymatic Chromatin IP Kit (Magnetic Beads) (Cell Signaling Technology, 9003) in accordance with the manufacturer's instructions and with reference to the method described by Xu et al.[54] Anti-β-CATENIN antibody was used for immunoprecipitation. Briefly, 50 mg of P7 brain tissue per group was cross-linked with 1% paraformaldehyde at room temperature, and chromatin was sonicated into fragments of 150–400 bp using an ultrasonic processor. A 10% aliquot of the sheared chromatin was set aside as the input fraction. Rabbit anti-β-CATENIN antibody, normal rabbit immunoglobulin G (as a negative control), and Histone H3 (D2B12) XP Rabbit Monoclonal Antibody (as a positive control) were added to the chromatin, followed by incubation at 4°C overnight. Chromatin-protein complexes were immunoprecipitated

with protein G magnetic beads. Cross-linking was then reversed by incubation with proteinase K at 65°C for 30 min, and DNA was purified using the DNA purification kit included in the ChIP kit. The eluted DNA was subsequently subjected to PCR, and the primers used for ChIP-PCR are listed in Table S1.

### TUNEL assay

For apoptotic cell detection, TUNEL staining was conducted with Roche TUNEL assay kit (Roche, 11684795910). Briefly, fixed brain tissue was permeabilized, followed by incubation with TUNEL reaction mixture at 37°C in dark. After nuclear counterstaining, apoptotic positive cells were observed and counted under fluorescence microscope.

### Immunofluorescence and immunohistochemistry

Mouse brain tissue samples were fixed overnight in 4% paraformaldehyde at 4°C, then transferred to 20% sucrose (Sangon, A610498-0005). After sedimentation, samples were placed in 30% sucrose and finally embedded in Tissue-Tek OCT Compound (Sakura Finetek) for cryoprotection. 14μm tissue sections were prepared for immunofluorescence and immunohistochemical staining. After sectioning, slides were washed three times with PBS, followed by antigen retrieval at 95°C (Sangon, E673001) for 25 min. After cooling to room temperature, slides were washed three times with PBS. Tissue was blocked with 5% goat serum at room temperature for 1 h, then incubated with primary antibody overnight at 4°C. The next day, wash three times with PBS, add fluorescently labeled secondary antibody and DAPI, incubate in the dark for 1 h, wash three times with PBS again, cover with Mowiol mounting medium, and observe and photograph under a fluorescence microscope. Antibodies used for immunofluorescence and immunohistochemistry are listed in key resources table. For immunohistochemistry, after antigen retrieval, incubate with 3% $H_2O_2$ solution at room temperature for 30 min before proceeding with blocking and primary antibody incubation. The next day, add HRP-labeled secondary antibody and incubate at room temperature for 1 h. After washing with PBS, add DAB chromogen solution until a clear positive signal appears, then immediately terminate the reaction by washing with distilled water. Cellular immunofluorescence followed a similar protocol to tissue immunofluorescence but did not require antigen retrieval. Antibodies used in the experiment are listed in key resources table.

### RNA *in situ* hybridization

14 μm frozen tissue sections were air-dried. Digoxigenin (DIG)-labeled RNA probes were synthesized by *in vitro* transcription using T3/T7 RNA polymerases, diluted with hybridization buffer, and denatured at 85°C before use. The sections were hybridized with denatured DIG-labeled specific probes overnight at 60°C in a humidified and sealed chamber. After hybridization, the sections were thoroughly rinsed with wash buffer and blocked with 10% heat-inactivated sheep serum at room temperature for 1 h. Subsequently, the sections were incubated with anti-DIG-alkaline phosphatase antibody (Roche, 11093274910) overnight at 4°C. The color reaction was developed using an NBT/BCIP detection kit (Roche, 11681451001). Finally, the sections were observed, and images were captured using a Leica DM6B microscope.

### qPCR

Following PBS perfusion of mouse cerebral cortex, tissue was rapidly frozen in liquid nitrogen. RNA was extracted per manufacturer instructions (TAKARA, 9108) and reverse transcribed to cDNA (Vazyme, R312-02). PCR systems were prepared according to reagent supplier protocols (Vazyme, P222-02) and analyzed using a Biorad CFX 96 instrument. Primary astrocytes and oligodendrocytes were washed with PBS in culture dishes, directly treated with Trizol, and processed as described above. Primer sequences are detailed in Table S1. Relative expression was calculated using the $2^{-(\Delta\Delta Ct)}$ method with β-actin as the reference gene. Data are presented as mean ± SEM. Each group included 3 replicate wells, with 3 independent replicates ($n = 3$). Intergroup comparisons were performed using one-way ANOVA. P-values are labeled on the bar charts.

### Western blot

Experimental methods were performed as previously described.[52] Briefly, cells or cerebral cortex were lysed and total protein was extracted. Proteins were separated by SDS-PAGE electrophoresis, transferred to PVDF membranes, and non-specific binding sites were blocked with 5% milk or BSA. Primary and secondary antibodies were added for incubation, followed by ECL chemiluminescence (Fdbio, FD8000) detection. Antibody information is provided in key resources table.

## QUANTIFICATION AND STATISTICAL ANALYSIS

Data analysis in this study was performed using GraphPad Prism 8.4. Data were analyzed using one-way ANOVA with Tukey's multiple comparisons for multiple groups, and unpaired Student's *t* test was used for two groups. The data are presented as mean ± SEM. The value of $p < 0.05$ was considered statistically significant. These statistical details of experiments can be found in the Figure legends.